Modeling and Control of a Fixed Wing Tilt-Rotor Tri-Copter

Alexander Summers

A thesis
submitted in partial fulfillment of the
requirements for the degree of

Master of Science in Aeronautics and Astronautics

University of Washington

2017

Reading Committee:

Kristi Morgansen, Chair

Eli Livne

Program Authorized to Offer Degree:
Department of Aeronautics and Astronautics

University of Washington

Abstract

Modeling and Control of a Fixed Wing Tilt-Rotor Tri-Copter

Alexander Summers

Chair of the Supervisory Committee:
PhD Kristi Morgansen
Aeronautics and Astronautics

The following thesis considers modeling and control of a fixed wing tilt-rotor tri-copter. An emphasis of the conceptual design is made toward payload transport. Aerodynamic panel code and CAD design provide the base aerodynamic, geometric, mass, and inertia properties. A set of non-linear dynamics are created considering gravity, aerodynamics in vertical takeoff and landing (VTOL) and forward flight, and propulsion applied to a three degree of freedom system. A transition strategy, that removes trajectory planning by means of scheduled inputs, is theorized. Three discrete controllers, utilizing separate control techniques, are applied to ensure stability in the aerodynamic regions of VTOL, transition, and forward flight. The controller techniques include linear quadratic regulation, full state integral action, gain scheduling, and proportional integral derivative (PID) flight control. Simulation of the model control system is completed for flight from forward to backward transition with mass and center of gravity variation.

TABLE OF CONTENTS

Page

Chapter 1: Motivation and BackGround 3
1.1 Motivation 3
1.2 A Brief History 3
1.3 Modern Times 5
1.4 Research 6

Chapter 2: Modeling 15
2.1 CAD Model 15
2.2 Longitudinal Dynamics 21
2.3 Gravity 22
2.4 Propulsion 22
2.5 Aerodynamics 23

Chapter 3: Control Strategy 28
3.1 Overview 28
3.2 Controller Goals 28
3.3 Control Concepts 32
3.4 VTOL Controller Synthesis 37
3.5 Transition Controller 41
3.6 Forward Flight Control 45
3.7 Transition Between Controllers 49

Chapter 4: Results 54
4.1 VTOL Controller: Hover Mode 54
4.2 VTOL Controller Climbing/Descending 66
4.3 Forward Transition 70
4.4 Backward Transition 78

4.5 Total Flight 83

Chapter 5: Conclusion 88

Bibliography 89

Chapter 1

MOTIVATION AND BACKGROUND

1.1 Motivation

The goal of the following thesis is to determine a flight control strategy for a hybrid vehicle that simplifies the transition from hover to forward flight and maintains vehicle stability with variation in center of gravity due to payload addition.

1.2 A Brief History

Hybrid vehicles started to surface during and after World War 2. Military demands started off the evolution of the hybrid aircraft; a vehicle capable of covering large distance quickly while still maintaining the ability to hover and land vertically, offered large opportunities in troop transport and payload movement. All these devices relied on pilots as the primary control system but, due to the strong non-linearity of the system, piloting hybrid aircraft was difficult for even experienced pilots. The developments of the concept however were of sufficient interest to the commercial and military manufacturers of the time that conceptual designs continued to be developed in theory. The conceptual designs ranged largely in the number of propellers, the manner in which vertical lift is achieved, and many other configuration aspects. Unfortunately few of the early design were manufactured for testing and even fewer made it into the intended industry[1].Two vehicles that were introduced into industry on a large scale are the Boeing V-22 Osprey and the Bell Eagle Eye, seen in Figure 1.1 and 1.2. Figures 1.3, 1.4, and 1.5 show examples of other conceptual and test designs.

Public perception of hybrid vehicles was poor even with these successful models. The benefits of a hybridized vehicle were weighed largely against the lack of stability of the sys-

Figure 1.1: The manufactured and operated Boeing V-22 Osprey [20].

Figure 1.2: The manufactured and operated Bell Eagle Eye[20].

Figure 1.3: The hybrid vehicle design of the DOAK Model 16 [1].

Figure 1.4: The conceptual design of the Boeing VZ-2A[1].

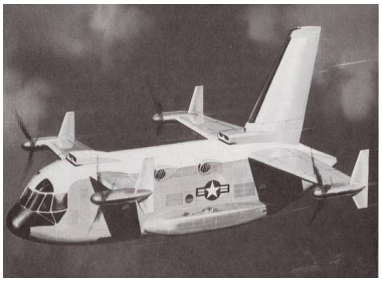

Figure 1.5: The conceptual design of the Douglas Model D-29 a hybrid aircraft [1].

tem, the difficulty in piloting, and the subsequent dangers posed to the crew. The models remained in operation despite the negative perceptions. The following quote from Congress describes the government perception in the context of the early 2000s [2].

> "Critics of the V-22 have questioned its affordability and argued that its performance would not justify the cost of procuring this new aircraft in the quantity

projected. Also, in light of several accidents, and a reported cover-up, critics argue that the tilt-rotor technology is too risky, while supporters contend that risks are being adequately addressed under a revamped program."

1.3 Modern Times

More recently the commercial market has been expanding rapidly into Unmanned Autonomous Vehicles (UAV). The possible applications continue to expand as hardware becomes more compact and weigh less, higher computational speed and storage become more available at lower cost levels, and energy storage and miniaturization evolve. The applications are varied across multiple industries; for example UAVs have been applied to surveillance, crop imaging, crop dusting, payload spraying, firefighting , and delivery systems for small parcels and packages [3, 4]. The potential is large, and the market opportunity is present. Start-ups to large companies are participating in the UAV trend.

Of the popular air-frame designs used in current applications, there are two main design types applied for UAV in industry, hovering/helicopter and fixed wing. Each has its own advantages and disadvantages. With a fixed wing aircraft, the efficiency of thrust is applied more effectively to maintain altitude. The fixed wing aircraft has a much larger range of operable distance as compared to a hover configuration with all other thing equal. However, fixed wing aircraft have restrictions on takeoff and landing. Some form of runway is required where flight velocity can be achieved and lost. The 'runway' can be introduced by various schemes including launchers and rapid propulsion devices for takeoff; and catching devices, such as sets or hooks [5], for landing. The runway requirement means maintenance, large flat areas, exterior structure (if a catching or launching system is required), and, depending on the complexity of the system, education.

Alternatively the use of hovering/helicopter configurations can be applied with advantages and disadvantages that contrast symmetrically with a fixed wing device. The advan-

tages of a hovering configuration include the ability to vertically takeoff in dense urban or agricultural areas, maneuver quickly in 3D, and land in a small footprint without external assistance. Unfortunately, the use of pure thrust to maintain altitude is highly inefficient and results in shorter flight time and smaller range, as compared to similar fixed wing devices under the same power constraints.

Integration of technology into societies is continuing to rapidly evolve. New ideas will continue to spring up, and old ideas may become viable again. This thesis is motivated by the benefits a hybrid vehicle would hold in the UAV aviation industry. The application of hybrid vehicles to meet the desired properties of range, flight time, efficiency, vertical takeoff and landing, and 3D maneuvering capabilities show great potential with current applications and technology. Agriculture based UAV could be simplified to require no structure dedicated to 'runway' or time commitment of an owner to set up, launch, and recover a device. Delivery UAV could require less charging intervals, larger flight range, and quicker delivery times. All these traits offer improvements in cost and performance.

1.4 Research

Research into hybrid vehicles has been around since the mid-1990s. The focus of much of the early work was based purely on investigating the modeling of the vehicle. Following the increase in availability of more powerful on-board computers, a focus toward autonomous designs began to increase in the early 2000s. Application of control system in both the linear and non-linear schools of thought were, and continue to be, applied around hybrid configurations.

1.4.1 Conceptual Designs

Hybrid conceptual designs maintain a large variation historically and currently. There is variation in how thrust is applied and vectored, variation in the number of thrust points ap-

plied, and differences in the method of transition between hover and forward flight. Designs that are similar in appearance actuate their control surface in different manners to achieve the same goals. The differentiation shows a lack of perfected method .By generalizing, the hybrid conceptual designs can be simplified to four main configurations corresponding to their number of thrust inputs.

Single Propeller Designs

Single rotor designs achieve vertical lift by making use of one propeller providing thrust. Examples of this type of vehicle can be seen in [8] and [9], and images of single propeller hybrid vehicles can be seen in Figures 1.6 and 1.7. To achieve vertical takeoff and landing from a ground level start, designs may be manufactured to support a vertical sitting orientation. These configurations are commonly known as tail sitters. There are alternatives to the sitting configuration fro single propeller devices. A single prop may also perch upon a vertical surface as the start point for flight as an example.

Transition, being the act of converting from hover to forward flight, occurs by means of thrust and aerodynamics flaps in a single propeller configuration. In a purely thrust based transition, vertical velocity (forward velocity in the body frame) increased due to thrust and flaps are applied to create a pitching moment, turning the vertical velocity into horizontal velocity. Alternatively the increase in velocity can be the result of gravitational force. Transitioning by means of reducing thrust and falling (gaining flight speed due to gravity) combined with aerodynamics control flaps is applicable to the same end.

As a note a net torque is created by the use of a single propeller. The rotational moment created by this torque is commonly canceled by the application of aerodynamic flaps operating within the thrust airflow.

Figure 1.6: A top view of a tail sitter conceptual design[8].

Figure 1.7: The Stanford perching UAV transitioning to vertical flight [9] .

Dual Propeller Designs

Examples of dual propeller designs can be seen in Figures 1.8 and 1.9. Dual propeller designs apply two wing-fixed propellers for vertical and horizontal thrust. The rotors have the ability to rotate in the pitch direction allowing for a changing of the thrust direction within the pitch plane. Transition is achieved using by tilting the propellers to provide acceleration vertically and horizontally from takeoff.

The primary difficulty with dual propeller vehicles is the need to maintain pitch equilibrium during operation. One method to maintain pitch balance is the use of aerodynamics flaps to create an angle of attack that counters thrust pitch with aerodynamic pitch [10]. This method of transition may require a skewed vertical takeoff. If a skewed take off is not desired, motion of the center of gravity by an actuator can allow for proper balancing of pitch moment[11].

Tri-Copter Designs

Examples of tri-rotor configurations can be seen in Figures 1.10, 1.11, and 1.12. Tri-propeller device perform in a similar manner to dual propeller devices. The addition of a

Figure 1.8: A dual propeller conceptual device [10].

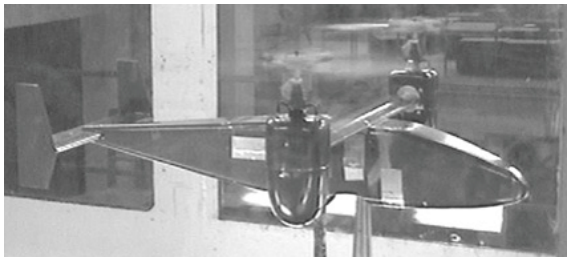

Figure 1.9: A manufactured dual propeller device undergoing wind tunnel testing [11].

third propeller allows pitch stability to be achieved through thrust. Applying three point of thrust allows for a simpler vertical takeoff and landing maneuver as compared to the single and dual propeller configurations.

Transition is achieved by tilting forward propellers that accelerate the hybrid craft while still providing vertical lift through thrust. A combination of tail thrust and elevator deflection maintain pitch equilibrium during this time. The tail thrust and elevator are redundant and it is possible to consider the use of both independently as well as blended. Blended dynamics have been investigated by way of cost functions to determine a trajectories with a combination of the elevator and tail thrust[14].

The presence of a third thrust inputs also affects system dynamics. The third propeller creates coupling of longitudinal inputs and lateral dynamics. Lateral dynamics and control are considered an independent control design problem in some research literature [11, 14]. Lateral control will not be discussed in this thesis.

Figure 1.10: The HARVEE design model of Arizona State University[14].

Figure 1.11: A tri-rotor with propellers off applied forward of the wing [13].

Figure 1.12: A modified RC plane for tri-rotor configuration [12].

Quad Propeller Design

Examples of the quad propeller style are seen in Figures 1.13 and 1.14. The quad propeller design applies four points of thrust symmetrically about the center of gravity. This design is similar in many respect to commercial quadcopters. Vertical takeoff and landing as well as 3D maneuvering are completed with thrust from the four propellers. With equal power applied to each propeller, the equilibrium of pitch and all other moment values are maintained. To achieve transition, the craft symmetrically tilts the propellers forward to increase flight velocity while maintaining altitude through thrust. A second wing is commonly added to provide aerodynamic lift and a mounting point[16, 17].

Figure 1.13: A quad-rotor design using an aerodynamic tail [16].

Figure 1.14: A quad-rotor design without stabilizing tail[17].

1.4.2 Modeling

Papers concerning the modeling of hybrid vehicles have been produced since the end of World War 2 [18, 19]. These papers demonstrate research into extensive wind tunnel modeling to determine the aerodynamic qualities of such a craft. Though it is typical to complete hand calculations as a basis for conceptual design for fixed wing aircraft, the usage of aerodynamic hand calculations fail in large degree when the applications are highly non-linear. The majority of the work thus proceeded with wind tunnel models to create descriptions of the aerodynamic characteristics of hybrid craft. Determination of airfoil lift and drag from zero to 180 degrees was completed in this manner.

Following the early 2000s, application of fluid dynamic programs to determine the aerodynamic forces was applied in addition to wind tunnel testing. The use of programs such as DATCOM and simple panel codes allow for aerodynamic terms to be iterated quickly and electronically[6],[7] before physical models are built. High level fluid dynamics can be

applied to determine the non-linear flow over the total configuration in a much more quickly than iterative building. The result is an increase of simulated models as a basis for control in current research.

The tilt-corridor is a numeric graph describing the vehicle velocity and its current tilt angle. An example tilt-corridor can be seen in Figure1.15. In modeling the dynamics of tilt propeller vehicles descriptions of the tilt-corridor can surface[20]. This corridor can provide understanding of vehicle trajectory and express limits of performance. Descriptions of vehicle trajectories in the tilt-corridor can also act as a basis for the equilibrium input magnitude and mixing (in the case of the elevator and tail thrust) [14]. Conceptual design that include aerodynamic control forces during transition or use tilting wings commonly include a tilt-corridor investigation.

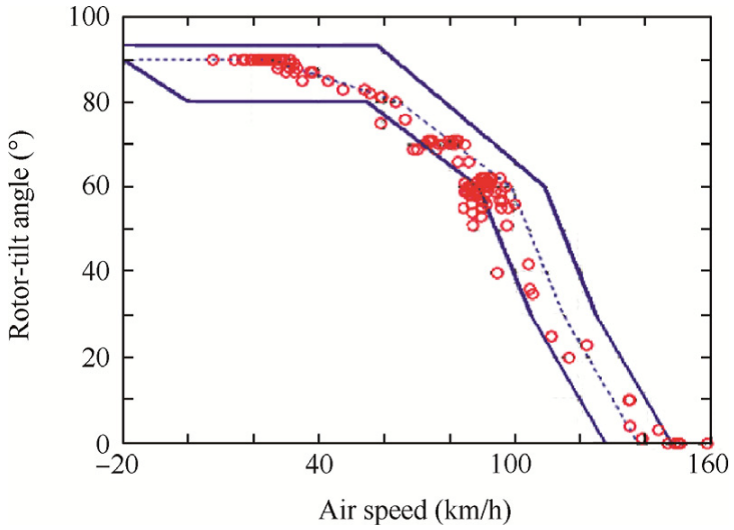

Figure 1.15: A generic tilt corridor describing flight speed at a given angle of attack [20].

1.4.3 Control Methodologies

Control techniques are varied largely in the control schemes for the different configurations. Difficulty in control designs stem from the large non-linearity of the system dynamics, the under-actuated nature of the plant, and the presence of coupled and repetitive inputs. This combination of issues make development of control techniques non-trivial in many respects and allows for control strategies to exist. Linear or non-linear control methods can be applied for the similar configurations as a result. The types of strategies employed in current research can be roughly generalized as follows.

Proportional gains can be applied in combination with gain scheduling to achieve non-linear control. Gain scheduling over variable parameters allows for interpolation of fixed gains, determined along this parameter, to achieve stability. Flight velocity is commonly the varied parameter, and scheduling of the gain variation occurs in reference to its magnitude. The gain choices can be found by iteration and optimization of a fixed structure controller [17] as well as through full state methods[10]. Proportional gains can be limited in that their tracking error performance. Poor error tracking leads to possible instability with the addition of model uncertainty. Use of H infinity synthesis controllers can be applied when robustness is a concern [14]. Depending on the controller structure used, the gains created via H infinity synthesis can include both proportional and integral gains.

Control applications surrounding various forms of PID control are commonly applied to hybrid vehicles. 'Virtual control inputs' can be created in tandem with PID controllers to achieve translation, altitude, and attitude control. These 'virtual control inputs' are high level (altitude, attitude) controller that are converted to low level (forward thrust, tail thrust) control inputs by means of a transformation matrix[21, 22, 23]. PD and PID controllers are combined with non-linear control methodology when used in transition. Non-linear methodologies that have been applied with PD/PID control include neural networks,

nonlinear back-stepping, sliding mode control, and various other adaptive control methods [12, 23, 24, 25]. As a note weight-compensated PID controllers are frequently applied for altitude control regardless of whether the remaining control strategy is based on PID.

The remaining work is spread out among miscellaneous methodologies that otherwise lack any commonality with other work. Adaptive control is applied to the strategy of transition in [9, 26, 27]. Controllers can be configured with polynomial methods such as Eigen-structure assignment in [11] or singular value decomposition methods in [28]. The use of neural networks are also applied in various forms such as dynamic inversion [29, 38, 39].

There have been many simulated control hybrid systems but few built and tested. Of those aircraft built and tested there are still fewer that maintained control without the assistance of a pilot during transition. Advancements must be continued to improve the control system to allow use in commercial application.

The contribution of this thesis is to create a control strategy that can be applied generally to tri-copter designs, removes the need for trajectory planning during hover to forward flight phase of hybrid vehicle, and maintains stability of a vehicle with variation in center of gravity due to the addition of a payload mass.

Chapter 2

MODELING

The following sections describe the conceptual CAD model and non-linear dynamics for a fixed wing tri-rotor configuration. A CAD model is created and iterated with an aerodynamic panel code to create a generic aircraft model for simulation. The non-linear dynamics to be applied for the 3 degree of freedom model will include gravitational, aerodynamic (both in VTOL and forward flight mode), and propulsion forces.

2.1 CAD Model

To create a model with realistic geometry, weight, and inertia, a conceptual model of a hybrid type vehicle was conceived and modeled using a CAD program.

2.1.1 Key Features

The conceptual model applies a set of design features based on previous configurations seen in the literature review. The chosen features, their reasoning, and the effect they have in the derivation of the non-linear dynamics are discussed in the following list.

Fixed Airfoils: The chosen design has fixed (non-tilting) airfoils at a set incidence of zero degrees. The fixed airfoils are used purely for forward aerodynamic lift and stability. The airfoils are modeled as NACA 0012, symmetric, airfoils with no dihedral angle or sweep. The choice of symmetric airfoil is made for simplicity and has the benefit of zero base aerodynamic forces. The zero base aerodynamic forces allows for aerodynamic stability of the aircraft to support a zero angle of attack during transition should aerodynamic stability

derivatives be stable.

The choice of wing fixation was made under the assumption that the drag induced in the vertical direction would be negligible in comparison to the drag felt at high wing tilt angles in forward flight. As well, the complexity in modeling and control are reduced by a fixed wing configuration.

In terms of the non-linear dynamic derivation, fixed wings will create a drag force and moment in VTOL. VTOL aerodynamics of the airfoils are considered perpendicular flat plate drag sources (a drag coefficient of 1.28). Forward flight will not see the flat plate drag and the airfoil will be assumed in a linear range of aerodynamics angle of attacks (the airfoil angle of attack will remain between negative ten and positive ten degrees).

Tri-Rotor Configuration: The chosen design utilizes a three propeller configuration. The propellers are distributed along the aircraft with two forward propellers (having a common tilt and equidistant from the plane of symmetry) placed on the forward airfoil and the third propeller fixed at the tail, along vertical body-axis. This configuration was chosen due to its ability to maintain VTOL equilibrium with pure thrust alone.

A quad rotor design was considered for its ability to maintain thrust based VTOL equilibrium as well. The quad rotor design model requires four symmetric propellers about the center of gravity. The fourth motor can be seen as redundant and the commonly applied 2nd wing structure incites dirty airflow when in forward flight. The decreased efficiency and the presence of more redundancy removes a quad rotor type configuration from consideration in this thesis. The modeling of the craft will consider 3 points of thrust as inputs.

Ducted Propellers: The finalized model makes use of ducted rotors. This increases safety (a valid design criteria should the aircraft be used in densely populated areas) and

the ducted rotors allow for more efficient flow. This efficiency is gained by avoiding flow interference that would occur between the open propeller airflow with its adjacent airfoil. In terms of dynamics derivation, thrust will be modeled as independent of thrust angle.

Low Aspect Ratio: The aircraft will maintain a thick chord in comparison to its span. The choice of low aspect ratio is with respect to the expected application of intercity payload transport. Use within a dense city area will restrict vehicle width, removing the possibility of more efficient high aspect ratio airfoil. The total span and length of the conceptual design are similar in nature to the circumference of a commercial octocopter.

Aerodynamic coefficient iterations, and the resulting aerodynamic simulation coefficients, were completed with the low aspect ratio as a design point.

Large Diameter Fuselage: The designed conceptual model includes a large diameter fuselage. The large diameter fuselage was chosen to with the intention of efficient payload storage. Storage of payload in the interior avoids inefficiency created by an exterior payload drag. The coefficients of drag for packaging shapes such as 3-D boxes in particular are quite large.

For modeling of the dynamics, interior payload storage means drag aerodynamics are purely based off the exterior geometry.

2.1.2 CAD Model

Applying the above features, and iterating in conjunction with an aerodynamic modeling program to achieve aerodynamic stability, results in the following CAD model seen in Figure 2.1, and the finalized geometric quantities can be seen in table 2.1.

Table 2.1: The geometric quantities for the conceptual vehicle.

Part	Value	Unit
Fuselage		
Fuselage Length	0.95	m
Fuselage Diameter	0.3	m
Wing		
Wing Leading Edge X position	0.54	m
Wing Span	1.6	m
Wing Chord	0.3	m
Wing Planform Area	0.48	m^2
AR	5.33	
Horizontal Tail		
Hor. Tail Leading Edge X position	1.7	m
Hor. Tail Span	0.7	m
Hor. Tail Chord	0.3	m
Hor. Tail Planform Area	0.21	m^2
Vertical Tail		
Ver. Tail Leading Edge X position	1.7	m
Ver. Tail Half Span	0.3	m
Ver. Tail Chord	0.2	m
Ver. Tail Planform Area	0.06	m^2

Part	Value	Unit
Center of Gravity		
X position	0.67	m
Y position	0	m
Z position	0	m
FWD Prop 1		
X position	0.54	m
Y position	0.89	m
Z position	0	m
FWD Prop 2		
X position	0.54	m
Y position	-0.89	m
Z position	0	m
Tail Prop		
X position	1.4	m
Y position	0	m
Z position	0	m

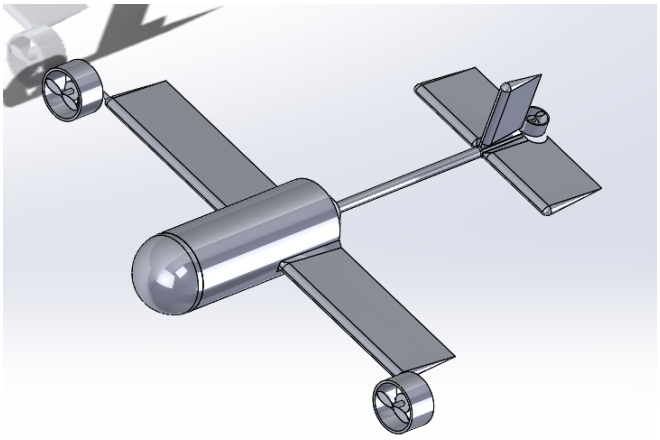

Figure 2.1: The conceptual design model of a VTOL/forward flight tri-rotor fixed wing configuration.

In addition to geometric quantities, modeling of the masses was completed. All structural components were approximated as lightweight material, such as carbon fiber-foam sandwich structure, and carbon fiber tubing. The index of vehicle components masses can be seen in Table 2.2.

The CAD model also provides a means to estimate more direct inertia values. The inertia about the Y-axis is thus determined to be 10.69 $\frac{Kg}{m^2}$ by means of the CAD model. This inertia will act as the base inertia for longitudinal rotation dynamics. Should the base design carry a payload, there will be variations of the center of gravity that result in an altered inertia. Modeling of the change of inertia with varied CG is completed based off point mass inertia assumptions and the parallel axis theorem taking the final form

$$I_{yy} = I_{yy0} + I_{yyVar} \tag{2.1}$$

$$I_{yyVar} = X_{cgVar}^2(m_0 + m_{Var}) + (m_{Var}\frac{m_0 + m_{Var}}{m_{Var}X_{cgVar}}^2). \tag{2.2}$$

Table 2.2: The mass properties of the hybrid conceptual vehicle.

Part	**Mass(Kg)**
Fuselage	6.5
Forward Engine(Individual)	1
Wing Half	1
Hor. Tail Half	0.5
Ver. Tail	0.5
Tail Prop	0.75
Tail Pipe	1.5
Payload	4.5
Unloaded Weight	***13.5***
Loaded Weight	***18***

2.2 Longitudinal Dynamics

Modeling and control will occur for the longitudinal dynamics of the hybrid vehicle and use a 3 DOF basis. The choice of the longitudinal plane, as opposed to both longitudinal and lateral planes, is due to the main concerns of transition pertaining to gravity, the effect of which is namely felt in the longitudinal plane.

The following assumptions are made for the longitudinal 3 DOF dynamics.

1. **Flat Earth Assumption:** The curvature of the earth will be ignored.

2. **Sea-Level**: The aerodynamics will be assumed to occur in constant air density. The air density will be assumed sea-level, $\rho = 1.225\frac{Kg}{m^3}$.

3. **Rigid Body**: The airframe is considered rigid. Flexible structure dynamics are ignored.

4. **Linear Aerodynamics**: The aerodynamics of the aircraft in the forward flight regime assume linear α range. Angle of attack will remain within the range from negative ten to positive ten degrees.

5. **Fixed Mass and CG**: Mass and CG variation are instantaneous and constant at the moment of takeoff. The payload addition is assumed to have a static nature.

The standard body-fixed 3 DOF dynamic equations

$$\begin{bmatrix} m(\dot{u} + qw) \\ m(\dot{w} - qu) \\ I_{yy}(\dot{q}) \end{bmatrix} = \begin{bmatrix} F_{AX} + F_{Gx} + F_{Px} \\ F_{AZ} + F_{GZ} + F_{PZ} \\ M_A + M_P \end{bmatrix} \tag{2.3}$$

are applied [30] with the above assumptions.

The change of non-body axis states Euler angle θ and altitude are described by

$$\begin{bmatrix} \dot{\theta} \\ \dot{h} \end{bmatrix} = \begin{bmatrix} q \\ u\sin(\theta) - w\cos(\theta) \end{bmatrix}. \tag{2.4}$$

The dynamic equations assume no coupling between the longitudinal and lateral dynamics. Lateral dynamic states v, β, p, r, ψ and ϕ are all considered to be zero. The aerodynamic effects of these terms will be considered negligible.

2.3 Gravity

Gravity is the main destabilizing factor during VTOL and early transition. Making use of the flat earth assumption, gravity is expressed by

$$F_G = \begin{bmatrix} F_{AX} \\ F_{AZ} \end{bmatrix} = \begin{bmatrix} -mgSin(\theta) \\ mgCos(\theta) \end{bmatrix}. \tag{2.5}$$

There is no moment applied due to gravity.

2.4 Propulsion

As stated previously, there are three thrust inputs present on the hybrid vehicle. The tail thrust is applied to the body fixed vertical axis pointing away from gravity with no tilt angle. The tail propeller is expected to utilize a maximum of 65 N in magnitude, and the tail thrust force is assumed to be capable of both positive and negative thrust.

Each forward propeller can provide 100N of force in the direction of tilt. Limitations are set for the deflection of the rotor tilt. The rotor tilt shall remain within 0 to 180 degrees. This tilt angle range encapsulates rotation necessary for vertical and horizontal modes. These

limits allow for a large range of VTOL control efforts and allow for a fixed tilt of zero degrees in forward flight.

The propulsion forces and moments take the form

$$F_P = \begin{bmatrix} F_{PX} \\ F_{PZ} \\ M_P \end{bmatrix} = \begin{bmatrix} T_p \cos(dT) \\ -T_p \sin(dT) - T_t \\ X_{T_p} T_p \sin(dT) + X_{T_t} T_t \end{bmatrix}. \tag{2.6}$$

The variable dT is defined from the forward body axis. The definition of positive dT deflection can be seen in Figure 2.2.

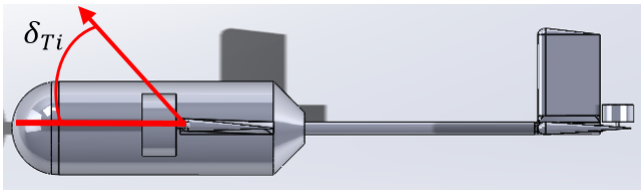

Figure 2.2: The definition of the zero value and positive deflection direction of the rotor tilt.

Variation of the center of gravity will cause the moment arms of the forward and tail thrust sources to be altered. The center of gravity variation will be applied to this configuration through adjustment of X_p and X_t in (2.6).

2.5 Aerodynamics

The aerodynamics for the given conceptual system are within two regimes, VTOL and forward flight. The aerodynamics equations of each region will be described below.

2.5.1 Forward Flight

The forward flight aerodynamic forces and moments in the longitudinal plane can be described by lift, drag, and pitching moment. The forces and moments are described with stability derivatives and base aerodynamics coefficients of the form

$$\begin{bmatrix} D \\ L \\ M \end{bmatrix} = \begin{bmatrix} (C_{D0} + \frac{C_L^2}{(\pi A_w e_w)}) q_d S_w \\ (C_{L0} + C_{L\alpha}\alpha + C_{Lq}q + C_{L\delta_e}\delta_e) q_d S_w \\ (C_{m0} + C_{m\alpha}\alpha + C_{mq}q + C_{m\delta_e}\delta_e) c_w q_d S_w \end{bmatrix}. \tag{2.7}$$

The aerodynamics forces from (2.7) are then put into the non-linear equations

$$F_A = \begin{bmatrix} F_{Ax} \\ F_{Az} \\ M_A \end{bmatrix} = \begin{bmatrix} -Dcos(\alpha) + Lsin(\alpha) \\ -Dsin(\alpha) - Lcos(\alpha) \\ M \end{bmatrix} \tag{2.8}$$

and describe the non-linear aerodynamics in the XZ Earth plane. Equation (2.7) also assumes that the efficiency factor e_w is equivalent to 1.

The forward flight coefficients of the conceptual vehicle were determined by means of an inviscid aerodynamic solver. The input geometry of the conceptual design can be seen in a panel based model format in Figure 2.5.1.

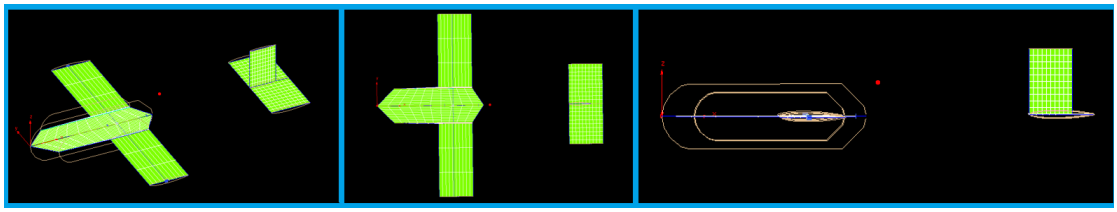

Figure 2.3: A 3-view representation of the aerodynamic model.

As stated previously, the airfoil incidences are zero degrees. The zero degree inclination allows the assumption that aerodynamic base coefficients are equivalent to zero (with the

exception of parasitic drag). With base coefficients equal to zero, the stability coefficients are used to linearly determine the aerodynamic forces and moments. The equation

$$C = C_{\alpha}\Delta\alpha + C_{q}\Delta q + C_{de}\Delta de. \tag{2.9}$$

describes the effect of each coefficient of the total aerodynamic force. The aerodynamic coefficients determined with the inviscid solver can be seen in Table 2.3.

Table 2.3: The aerodynamics stability derivatives determined from the invisid solver.

$C_{L\alpha}$	C_{Lq}	$C_{M\alpha}$	C_{Mq}	C_{Lde}	C_{Mde}
5.353395	0.040042	-0.73129	-0.11265	0.338847	-1.32495

The parasitic drag coefficient is not a determined quantity within many inviscid solvers. The parasitic drag coefficient is thus determined by means of the component build up method [31] seen for this configuration as

$$CD_0 = CD_W + CD_F\frac{S_F}{S_W} + CD_{HT}\frac{S_{HT}}{S_W} + CD_{VT}\frac{S_{VT}}{S_W}. \tag{2.10}$$

Table 2.4 describes the component drags considered for each major aerodynamic component of the conceptual design and the final parasitic drag coefficient.

The addition of mass and resulting movement of CG will alter the aerodynamics coefficients in Table 2.3, such as $C_{M\alpha}$ and C_{Lq}. The coefficients and their adjusted values can be seen over a range of -0.1 m to +0.1 m variation from the center of gravity in Table 2.5. The non-linear model for the conceptual design will include look-up Tables describing the coefficients as a function of the variation of the CG.

Table 2.4: Component drags of various components of the conceptual aircraft.

Component	$CD_i \frac{S_i}{S_w}$
Fuslage	0.01175
Wing	0.01
Hor Tail	0.004
Vert Tail	0.001
Total CD	**0.02675**

Table 2.5: A description of the alteration in aerodynamic coefficients due to CG variation.

X_{CG} **Variation**	$C_{L\alpha}$	C_{Lq}	$C_{M\alpha}$	C_{Mq}	C_{Lde}	C_{Mde}
-0.1	5.353395	0.050743	-2.5157	-0.13102	0.338847	-1.43794
-0.05	5.353395	0.045392	-1.6235	-0.12095	0.338847	-1.38147
0	5.353395	0.040042	-0.73129	-0.11265	0.338847	-1.32495
0.05	5.353395	0.034691	0.160911	-0.10614	0.338847	-1.26848
0.1	5.353395	0.02934	1.053229	-0.10141	0.338847	-1.21202

2.5.2 VTOL Aerodynamics

The aerodynamic equations for VTOL assume forward velocity is small in magnitude to vertical velocity and will be neglected. The only aerodynamic effect in VTOL mode is thus vertical velocity induced drag and moment. The majority of aerodynamic forces are assumed to be caused by flat plate drag of the airfoils. Drag caused by the fuselage and tail pipe will be neglected. The VTOL aerodynamics are described as

$$\begin{bmatrix} F_{Ax} \\ F_{Az} \\ M_A \end{bmatrix} = \begin{bmatrix} 0 \\ -\frac{0.5CD_{fp}\rho_{inf}S_w w^2(\frac{S_h}{S_w}+S_w)}{m} \\ \frac{0.5CD_{fp}\rho_i nfS_w w^2(\frac{S_h}{S_w}X_H+S_w X_w)}{I_{yy}} \end{bmatrix}. \tag{2.11}$$

Chapter 3

CONTROL STRATEGY

3.1 Overview

As mentioned in previous section, a hybrid vehicle offers difficulties in many areas of control design. The difficulties revolve around the large range of flight conditions in which operation occurs and the nonlinear dynamics associated with these regimes. The plant itself is an under-actuated system with more states to be controlled than inputs available for control. The inputs are strongly coupled with multiple inputs controlling the same state. Some inputs can be being entirely ineffective in a flight space (elevator).

Control system design will focus on creating discrete controllers for the vertical takeoff and landing regime, transition regime, and the forward flight regime respectively. To achieve controller synthesis in the required regimes, redundant inputs will be designated off and certain states will be considered disturbances.

The approach to forward transition from VTOL to forward flight is to use thrust based lift to provide control in the VTOL and transition stages and then switch to aerodynamic lift based control in the forward flight stage. The reverse sequence will occur for backward transition from forward flight to VTOL.

3.2 Controller Goals

The plant model experiences dynamics in two different aerodynamics regimes, hover and forward flight. The two are connected by transition dynamics which will apply the same

aerodynamics coefficients as forward flight but will operate in lower velocities. Three controllers will be applied for the total flight envelope in this thesis to guarantee stability during operation in both VTOL and forward flight as well the connecting regime. The three controllers and their necessary goals for each control regime are described below.

3.2.1 VTOL

The vertical take-off and landing controller is required to ensure stability in all states. These states include forward velocity, vertical velocity, pitch angle, and pitch rate. The expectation is that all states will remain zero with the exception of w, vertical velocity. The altitude state is dependent purely on the aforementioned states and will be neutrally stable should θ and w be controlled to their desired values of zero and remain stable. If the vehicle thrust is pointed away from gravity and all torques and forces are in equilibrium, the altitude must be constant.

The expected operation involves the vehicle taking off and landing in building dense areas where forward velocity would likely incite collisions. A requirement for zero forward velocity will be imposed. Forward velocity also requires rotor tilting that in turn increases the thrust load requirements to maintain hover or climb velocities. The application of non-zero forward velocities will be applied only when a transition altitude is achieved.

The requirement is set that the VTOL controller must be effective over a vertical velocity range of negative five to positive five meters per second. The vertical motion of a fixed wing aircraft will induce drag due to aerodynamics effects. The aerodynamic effects are largely ignored in much research for the VTOL regime but will be accounted for as flat plate drag of the airfoils in this thesis. The variation of vertical velocity to achieve a desired altitude will require controller effectiveness throughout a range of vertical velocities.

3.2.2 Transition

The stability requirements for the transition regime are very similar to the VTOL controller stability requirements. The requirements are altered however by considering the forward velocity, and its effect on other states, as a disturbance.

The stability requirements for the transition regime are stable vertical velocity, pitch angle, and pitch rate. The states will be controlled to zero for overall stability to be achieved. Altitude will be controlled toward a constant value during the majority of transition as well by means of stabilizing the states w, q, and theta. The argument is discussed in the VTOL section.

A requirement of zero vertical velocity is chosen with the desire of constant altitude and also with the desire of a zero angle of attack in forward flight. The desire of a zero angle of attack is due to the transition controller treating aerodynamic forces as disturbances. At zero angle of attack (for a symmetric aircraft with no incidence) aerodynamic forces are zero. The zero aerodynamic forces thus minimizes the disturbances, and the transition event requires less control effort. A zero angle of attack also increases the validity of the linear aerodynamic assumption during transition as well as avoiding a braking effect of the vertical tail.

The theta and pitch requirements act similarly to the zero angle of attack desire. Theta and pitch rotation set to zero avoid braking forces due to angled thrust, specifically the tail thrust which is fixed along the vertical body axis. Additionally the q and theta requirements guarantee that the vertical body axis is always pointing away from gravity. This pointing combined with no vertical velocity supports the goal of constant altitude as well as stabilizing the forward velocity. The forward velocity will be at least marginally stable due to the avoidance of gravity excitement (the effect of a non-zero theta) and the presence of drag.

The requirement that the transition control maintains a stable vehicle orientation as forward velocity is accelerated from zero to 50 meters per second (a speed within the viable flight envelope) is made. The acceleration period will employ a predetermined rotor tilt trajectory. The scheduled tilt removes the need for trajectory planning for all configuration of mass, CG, and their related inputs. A tilt schedule simplifies the forward acceleration and allows for a more general application of the controller to new systems. Having a controller design that creates a more amiable environment to the scheduled tilt is thus desired.

The requirement of removed redundancy by means of tail thrust pitch control only is set. The lift force will be purely generated by thrust forces. The removal of the elevator simplifies the redundancy of pitch control due to cross coupling of the elevator and tail fan. The elevator would also incite an angle of attack disagreeing with the zero angle of attack desires mentioned previously. As well the elevator is not very effective at low flight velocities.

3.2.3 Forward Controller

The forward controller holds the requirement of maintaining altitude following entrance into the flight envelope. Stability of the states, u, w, q, and theta are maintained with constant altitude flight as this is a steady level flight equilibrium.

The requirement of removed redundancy by means of elevator control only is set. A single control pitch input is needed for constant altitude in steady level flight. The elevator is far more efficient in forward flight and now has a larger control effect compared to the lower flight velocities of the transition regime.

The controller is desired to maintain stability throughout scheduled tilt and thrust manipulations. The forward flight controller is applied in the flight envelope at the flight velocity

of 50 meters per second. Transition in the forward flight regime will include multiple position of rotor tilts and thrust to meet the parasitic and induced drags. The controller needs to be able to manage the thrust and tilts for a successful transition.

3.3 Control Concepts

3.3.1 Full State Control

To create a linear controller for a general system the Jacobian method is applied to the non-linear equation of the system states and inputs about a chosen equilibrium point. The inputs used in linearization must be fed forward to the controller to maintain the expected equilibrium. The Jacobian method takes the first derivative of all states and inputs as a first order approximation of non-linear dynamics. The Jacobian method results in matrices A, B, C and D. The matrices are used to create a continuous linear time invariant system describing the non-linear mechanics of a hybrid vehicle for which a control scheme can be designed. The general state space form can be seen in equation (3.1)

$$\dot{x} = Ax + Bu; \quad y = Cx + Du \tag{3.1}$$

The first step of designing a linear controller is to determine the linear system properties. System properties of interest include whether control is achievable/necessary, the current stability type, and whether the system is observable.

The question of stability can be addressed by simply performing an eigenvalue test of the determined A matrix. Should any eigenvalue have a positive real portion the system is unstable. Eigenvalues are thus desired to have negative real portions. Control applications allow for a change in sign of eigenvalues and are desired in cases where stability requirement are not met.

The ability to stabilize the system revolves around the ability to control the states of the plant. The controllability of a given system can be determined by taking the controllability matrix

$$C = \begin{bmatrix} B & AB & ... & A^{n-1}B \end{bmatrix} \tag{3.2}$$

and determining its rank[35]. When the controllability matrix is full rank the system is controllable.

A similar method can be used to determine the observability of the CLTI system. The observability matrix is of the form

$$O = \begin{bmatrix} C & CA & ... & CA^{n-1} \end{bmatrix}' \tag{3.3}$$

and describes the ability to discern all the states from a set of observations [35]. If the observabilty matrix is full rank then all states are observable with the given output matrix C. In the following thesis work, the assumption is made that all states are observed and the plant is always fully observable.

Given knowledge of the system concerning stability, controllability, and observability progress can now be made to form a theoretic control system for the given CLTI system. To create a feedback controller for a given linear system, a stability matrix must be created based on the A and B matrices and used in conjunction with the Lyapanov stability function to create a feedback "K" matrix for which $(A - BK)$ will have negative real eigenvalues.

First, the A matrix must be manipulated to find a stability matrix by subtracting a constant multiplier of the identity matrix. This matrix and the B matrix for the given CLTI system are then used to solve for matrix W, via the Lyapanov Equation[35]. A K matrix can then be created using the B matrix and the newly found W matrix by applying

$$\bar{A} = \mu I - A \rightarrow \bar{A}W + W\bar{A}' = -BB'$$

$$\rightarrow P = W^{-1} \rightarrow K = \frac{1}{2}B'P. \quad (3.4)$$

Alternatively, with the given knowledge of the system concerning stability, controllability, and observability, a theoretic optimal control system can be created for a CLTI system.

One method to create an optimal controller is to solve the Linear Quadratic Regulator problem. The cost function for this regulator will take the form of

$$J = \frac{1}{2}x'_{tf}P_{tf}x_{tf} + \frac{1}{2}\int x'Qx + u'Ru \quad (3.5)$$

[36] and, specifically for this thesis, the form

$$J = \int x'Qx + u'Ru \quad (3.6)$$

will be applied.

In the cost equation J represents an associated cost of control. 'x' and 'u 'represent state and input. Q and R represent the cost weighting matrices for state and input control.

The Hamiltonian, otherwise defined as H takes the form

$$H = \frac{1}{2}(x'Qx + u'Ru) + \lambda_t A_t. \quad (3.7)$$

The Hamiltonian can be solved for an optimal input using minimization principles. By use of linear algebra, and some clever inference, it can be found the form of the optimal u (input) is

$$u = -C_t x; \quad C_t = R_t^{-1}B_t'P_t'. \quad (3.8)$$

The unknown matrix P in this formula can be found with knowledge of its end point P_{tf} (considered zero in this thesis) and the use of the differential Ricatti equation [36] of the form

$$\dot{P}_t = -A_t' P_t - P_t A_t - Q_t + P_t B_t R^{-1} B_t' P_t. \tag{3.9}$$

The time varying P_t matrix reaches a steady state value and can be approximated as a constant, resulting in a time invariant optimal controller.

3.3.2 Integral Action

Full state gains provide stability about a linearization point but do not necessarily imply zero tracking error. The ability to determine a steady state input while controlling state to zero error is very useful when alteration of the system CG and mass occur without modeling knowledge. A lack of CG and mass knowledge would be common in the case of UAV capable of transporting payload. The application of integral gain is thus a necessary requirement for a payload transportation and will be included in the full state control method.

The states space equations from (3.1) can be modified with integrators to adjust for system uncertainty and provide tracking of desired states. The process for augmentation is to introduce a new state 'z', where the relationship

$$\dot{z} = r - y = r - Cx \tag{3.10}$$

is held for the reference 'r' and the output 'y' [32].

The new state 'z' thus represents the integral of the error between the reference and output. Augmenting the previous A and B matrices to include the new variable results in

$$A^* = \begin{bmatrix} A_{nxn} & 0_{nxq} \\ -C_{qxn} & 0_{qxq} \end{bmatrix} \quad B^* = \begin{bmatrix} B_{nxm} \\ 0_{qxm} \end{bmatrix} \tag{3.11}$$

describing states and integrator dynamics ('q' represents the integrated state dimension, 'n' the states of the plant, and 'm' the input dimension).

With the augmentation of the linearization matrices, linear control theory can be applied to determine proportional and derivative gains. Using LQR or pole placement result in a gain matrix

$$K^* = \begin{bmatrix} Kp_{mxn} & Ki_{qxn} \end{bmatrix}, \tag{3.12}$$

with both proportional and integral gains.

It should be noted that the creation of the new states must also be represented in the Q and R matrices for LQR. As well there are limitation of the integrator augmentation in that the amount of states that can be tracked cannot be greater than the amount of inputs available.

3.3.3 Gain Scheduling

An industry approved method for control of a range non-linear dynamics is the use of gain scheduling. Gain scheduling itself is a generic term for the mapping together of linear control systems along a family equilibrium points in a non-linear regime.

The steps for gain scheduling are commonly simplified to its main points [33].

1. Create a linear parameter varying system describing the non-linear plant.

2. Determine a family of operating points

3. Create linear controllers for the family of equilibrium points.

4. Interpolate the controllers together and apply the total controller to the non-linear system.

The linear parameter varying (LPV) system is commonly created via linearization of the non-linear plant dynamics with the Jacobian method and leaving equilibrium values as general variables. Points of equilibrium are then determined at varied parameters of interest (found algebraically or numerically). Linear controllers designed for the LPV system can be of any form, but a consistent controller form will simplify interpolation. In the following controller synthesis interpolation via look up Tables with full state controller gains is applied.

3.4 VTOL Controller Synthesis

Linearizing the VTOL non-linear dynamics by way of the Jabcobian method results in the required matrices for designing a controller for the VTOL stage. The linear parameter varying systems in equation

$$A = \begin{bmatrix} 0 & -q & -w & -g\cos(\theta) \\ q & -\frac{CD_{fp}\rho_{inf}S(S_h+S_w)w}{m} & u & -g\sin(\theta) \\ 0 & \frac{CD_{fp}\rho_{inf}Sw(S_hX_H+S_wX_w)}{I_{yy}} & 0 & 0 \\ 0 & 0 & 1 & 0 \end{bmatrix}; x = \begin{bmatrix} u \\ w \\ q \\ \theta \end{bmatrix} \tag{3.13}$$

$$B = \begin{bmatrix} \frac{\cos(dT)}{m} & 0 & -\frac{T_p\sin(dT)}{m} & 0 \\ -\frac{\sin(dT)}{m} & -\frac{1}{m} & -\frac{T_p\cos(dT)}{m} & 0 \\ \frac{Z_{Tp}\cos(dT)+X_{Tp}\sin(dT)}{I_{yy}} & \frac{X_{Tt}}{I_{yy}} & \frac{T_pX_{Tp}\cos(dT)-T_pZ_{Tp}\sin(dT)}{I_{yy}} & 0 \end{bmatrix}; u = \begin{bmatrix} T_p \\ T_t \\ dT \\ de \end{bmatrix} \tag{3.14}$$

describe the linearized state and input dynamics for VTOL.

Taking the eigenvalues of A and B at a hover condition results in all zero eigenvalues. The zero eigenvalues represent a marginally stable system. Intuitively, if the linearized hover

condition were to hold true at all times the plant would be marginally stable. This truth holds for all case where linearization occurs about a zero theta. Linearizations about a non-zero theta can be seen to have eigenvalues similar to

$$\lambda = \begin{bmatrix} 0.0000 + 0.0000i & -0.1682 + 0.2407i \\ -0.1682 - 0.2407i & 0.2563 + 0.0000i \end{bmatrix}, \tag{3.15}$$

with positive and zero eigenvalues, the system is unstable.

In either case the desired stability results and convergence of states to a value is not achieved and a controller is thus desired. The controllability matrix is tested for rank and is found to be full rank and controllable.

For the VTOL case, integration of the two states w and theta are all that is required to meet our controller goals of stability. The forward velocity, u, will be stabilized about zero by proportional gains alone. The augmented A matrix will thus use

$$C_{int} = \begin{bmatrix} 0 & 1 & 0 & 0 \\ 0 & 0 & 0 & 1 \end{bmatrix} \tag{3.16}$$

to describe the integration state variables.

The Q matrix for the given states and integrators takes the form

$$Q = \begin{bmatrix} 1 & 0 & 0 & 0 & 0 & 0 \\ 0 & 100 & 0 & 0 & 0 & 0 \\ 0 & 0 & 1 & 0 & 0 & 0 \\ 0 & 0 & 0 & 100 & 0 & 0 \\ 0 & 0 & 0 & 0 & 100 & 0 \\ 0 & 0 & 0 & 0 & 0 & 100 \end{bmatrix}, \tag{3.17}$$

with the states w and theta, and their integration, having a large weighting. When mass is added or vertical velocity induces drag forces and moments these states will need to be

integrated to avoid tracking error. The forward velocity and pitch rate are stabilized by quick integration of w and theta, and are thus weighted with less importance.

The R matrix

$$R = \begin{bmatrix} 1 & 0 & 0 & 0 \\ 0 & 1 & 0 & 0 \\ 0 & 0 & 10 & 0 \\ 0 & 0 & 0 & 1 \end{bmatrix} \tag{3.18}$$

describes the weightings for the inputs. The R matrix for the VTOL controller puts a heavier weight on the tilt angle control. Large deviations of the tilt can lead to instability when the linear assumption breaks down. In addition the use of rotor tilt increases the thrust load of the vehicle to compensate for redirected thrust vectors which is inefficient.

Applying the augmented A, B, Q, and R matrices to the LQR problem and solving for gains results in a stabilizing controller. An example of eigenvalues created using this method with the hover condition are

$$\lambda(A^* - B^*K^*) = \begin{bmatrix} -8.3507 + 0.0000i & -0.8032 + 0.8995i & -0.8032 - 0.8995i \\ -0.7317 + 0.0000i & -0.3213 + 0.0000i & -0.5512 + 0.0000i \end{bmatrix}. \tag{3.19}$$

All eigenvalues are in the left half plane of the real-imaginary axis and thus all states, and their integrated errors, are stable and their error will converge to zero. As well the eigenvalues' magnitudes are not excessively large and control efforts are expected to not exceed input limitations.

A simulation of the perturbed linear system with the controller can be seen below in Figure 3.1.

The same method is completed for a range of vertical velocities from negative five to positive five meters per second. Points are chosen within this range and their equilibrium states

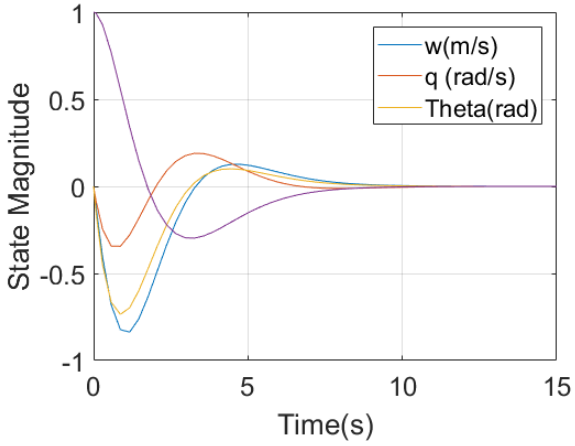

Figure 3.1: The perturbed response of the linear system with feedback control provided by LQR gains.

and inputs are solved for and added to LPV A and B matrices. The linear controllers are then created and interpolated at each point. The interpolation of the controller is completed by way of weighting function

$$C = \alpha C_1 + (1 - \alpha)C_2 \quad where \quad 0 < \alpha < 1. \tag{3.20}$$

In simulation, the interpolation is applied by use of look up tables following this weighting. The remainder of the full state control system design is to include equilibrium inputs of linearization as a feed forward controller inputs. These inputs are created from the unloaded model of the system for the VTOL controller but will be passed on to following transition controllers as discussed in the later switching section. Using the non-linear dynamics, the geometric factors, and aerodynamic coefficients from the modeling section, the feed forward inputs takes the form

$$\begin{bmatrix} T_p \\ T_t \\ dT \\ de \end{bmatrix} = \begin{bmatrix} 112.416 - 0.318887 * W.^2 * Sign(W) \\ 20.0192 - 0.222073 * W.^2 * Sign(W \\ \pi/2 \\ 0 \end{bmatrix} \tag{3.21}$$

for the unloaded case. The unloaded case will act as the starting point for all control inputs.

Note that when 'w' is equal to zero the hover equilibrium is found. The hover equilibrium is found to be 112 N applied between the forward propellers, and 20 N applied by the tail propeller. Both of the thrust forces are within the expected limitations mentioned in the propulsion section of modeling.

With the application of optimal full state feedback and gain scheduling, the goals for the VTOL controller are met. The states of the system are all stable, as can be seen by the negative real portions of eigenvalues. The addition of integrators guarantees stability and state tracking in the presence of model uncertainty. The gains scheduling gives stability throughout the range of desired vertical velocities. The stability of the non-integrated state of forward velocity will be kept stable about zero by proportional gains.

Demonstration of the VTOL controller applied to the non-linear system will be discussed in the simulation section of this thesis.

3.5 Transition Controller

A similar method to VTOL control is applied to the transition controller method. A linear parameter varying system is determined similar in nature to the hover LPV is created but the state of forward velocity is ignored. Previous work with neural networks PID control [12] has demonstrated the plausibility of a weight compensated hover controller to be

adjusted to achieve transition. The method using PID fails with poor knowledge of the CG, and is adjusted to full state control in this thesis.

The systems A and B matrix are seen in equation 3.22 and 3.23.

$$A = \begin{bmatrix} 0 & u & -g\sin(\theta) \\ 0 & 0 & 0 \\ 0 & 1 & 0 \end{bmatrix}; x = \begin{bmatrix} w \\ q \\ \theta \end{bmatrix} \tag{3.22}$$

$$B = \begin{bmatrix} -\frac{\sin(dT)}{m} & -\frac{1}{m} & 0 & 0 \\ \frac{Z_{Tp}\cos(dT)+X_{Tp}\sin(dT)}{I_{yy}} & \frac{X_{Tt}}{I_{yy}} & 0 & 0 \end{bmatrix}; u = \begin{bmatrix} T_p \\ T_t \\ dT \\ de \end{bmatrix} \tag{3.23}$$

Note that the input matrix B has two columns of zero. The rotor tilt angle is independently scheduled and is not considered a usable input to the system. The elevator deflection is also considered off due to its redundancy. The inputs are thus left blank in the input matrix.

The eigenvalues of this system are the same as in the hover condition. The eigenvalues demonstrate the same marginal stability about the equilibrium point, and the same instability at non-zero theta. A check for controllability of the system gives a full rank of the controllability matrix, three, and thus the system is controllable.

To achieve the controller goals mentioned above, w and θ will be the integrated values once more. The resulting integral C matrix takes the form

$$C_{int} = \begin{bmatrix} 0 & 1 & 0 & 0 \\ 0 & 0 & 0 & 1 \end{bmatrix}. \tag{3.24}$$

The states weight of the Q matrix takes the form

$$Q = \begin{bmatrix} 10 & 0 & 0 & 0 & 0 \\ 0 & 10 & 0 & 0 & 0 \\ 0 & 0 & 10 & 0 & 0 \\ 0 & 0 & 0 & 100 & 0 \\ 0 & 0 & 0 & 0 & 100 \end{bmatrix}. \tag{3.25}$$

with higher weights applied to the integrated states of w and theta. Quickly achieving and maintaining the desired w and θ equivalent of zero is a necessity for stability.

The R matrix takes the form

$$R = \begin{bmatrix} 1 & 0 & 0 & 0 \\ 0 & 1 & 0 & 0 \\ 0 & 0 & 1 & 0 \\ 0 & 0 & 0 & 1 \end{bmatrix}. \tag{3.26}$$

with all inputs equally weighted. The thrust inputs are equally responsible for maintenance of lift and moment control. The weighting for the elevator and tilt angle is irrelevant as these inputs will be considered independent of feedback.

The chosen Q and R matrices are then applied to the LQR problem and gains are determined. The eigenvalues for the tilt angle of 90 degrees are

$$\lambda(A^* - B^*K^*) = \begin{bmatrix} -0.7173 + 0.7246i & -0.7173 - 0.7246i & -0.4515 + 0.6878i \\ -0.4515 - 0.6878i & -0.8468 + 0.0000i & \end{bmatrix}. \tag{3.27}$$

The eigenvalues all have negative real portion and are thus stable. The magnitudes are small and the control effort is expected to stay within limitations. The resulting perturbed response of the system can be seen in Figure 3.2. Non-linear control response will be covered in the results section.

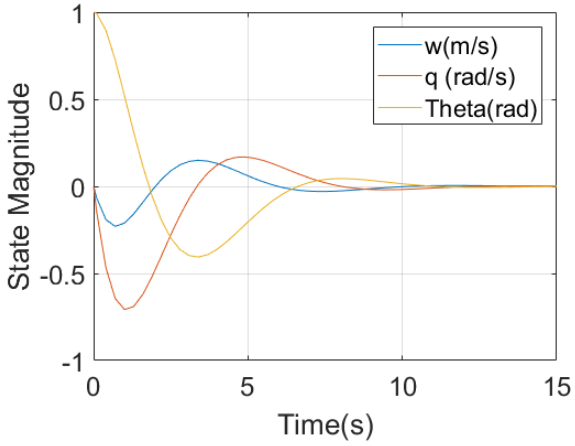

Figure 3.2: Perturbation response of the linear transition controller with determined LQR gains.

The gain scheduling approach is then applied with the varying parameter set to be the tilt angle of the rotors. The tilt angle during the transition stage operates between 70 and 90 degrees (vertical). LQR gain matrices are determined for a family of points within the tilt region and interpolated by the same weighting function as the VTOL controller (3.20).

The inputs for feed forward are based upon the equilibrium condition from hover. The equilibrium values learned from the prior hover stage are passed to the transition controller such that the form

$$\begin{bmatrix} T_p \\ T_t \\ dT \\ de \end{bmatrix} = \begin{bmatrix} T_{Peq} csc(dT) \\ T_{teq} \\ Scheduled \\ 0 \end{bmatrix} \tag{3.28}$$

is achieved. T_{Peq} and T_{teq} are the forward and tail thrust values when hover equilibrium with the VTOL controller. These values are dependent on the payload and CG variation. A new term '$csc(dT)$' can be seen included in the feed forward command as well. In implementation of the final controller, the thrust constants will be altered based on the current rotor tilt in

order to maintain a thrust equivalent to weight.

The goals for the transition controller have thus been met. Through the LQR method, proportional and integral gains have been determined which stabilize our three states of w, theta, and q. The integration ensures that the equilibrium inputs for w and theta stability are found and held. The tilt angle is left independent of feedback control, and is a scheduled quantity as desired and the elevator maintains a zero input with no feedback control.

3.6 Forward Flight Control

The general form of linearized forward flight system. This form is a common definition of the linear aerodynamics [30] is seen in (3.29) and (3.30).

$$A = \begin{bmatrix} X_u & X_\alpha - q & X_q - w & -g\cos(\theta) & 0 \\ q + Z_u & Z_\alpha & u + Z_q & -g\sin(\theta) & 0 \\ M_u & M_\alpha & M_q & 0 & 0 \\ 0 & 0 & 1 & 0 & 0 \\ \sin(\theta) & -\cos(\theta) & 0 & u\cos(\theta) + w\sin(\theta) & 0 \end{bmatrix}; x = \begin{bmatrix} u \\ w \\ q \\ \theta \\ h \end{bmatrix} \tag{3.29}$$

$$B = \begin{bmatrix} \frac{\cos(dT)}{m} & 0 & -\frac{T_p\sin(dT)}{m} & X_{de} \\ -\frac{\sin(dT)}{m} & -\frac{1}{m} & -\frac{T_p\cos(dT)}{m} & Z_{de} \\ \frac{Z_{Tp}\cos(dT)+X_{Tp}\sin(dT)}{I_{yy}} & \frac{X_{Tt}}{I_{yy}} & \frac{T_pX_{Tp}\cos(dT)-T_pZ_{Tp}\sin(dT)}{I_{yy}} & M_{de} \\ 0 & 0 & 0 & 0 \\ 0 & 0 & 0 & 0 \end{bmatrix}; u = \begin{bmatrix} T_p \\ T_t \\ dT \\ de \end{bmatrix} \tag{3.30}$$

The variables seen in the A and B matrices are dimensional aerodynamic derivatives. The aerodynamic coefficients and the flight condition discussed in the modeling section are the basis for these dimensional derivatives. The dimensional derivatives at the flight condition of 50 meters per second is given in Table 3.1.

Table 3.1: Dimensional derivatives at a steady level flight condition of 50 meters per second and α of two degrees.

Dimensinoal Derivative	**Value**
Xu	-0.07
Xalpha	1.621
Xq	0
Xde	0
Zu	-0.4133
Zalpha	-293.028
Zq	-0.0065
Zde	-15.57
Mu	0
Malpha	-15.05
Mq	-0.007
Mde	-24.75

The eigenvalues

$$\lambda = \begin{bmatrix} 0.0000 + 0.0000i \\ -2.9456 + 2.5478i \\ -2.9456 - 2.5478i \\ -0.0231 + 0.2818i \\ -0.0231 - 0.2818i \end{bmatrix} \tag{3.31}$$

can be seen plotted in Figure 3.3. A plot of the A matrix eigenvalues with variation of flight

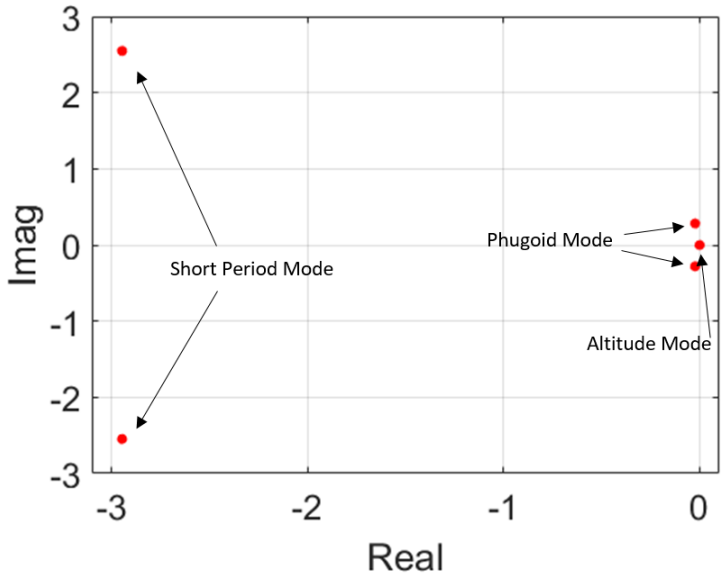

Figure 3.3: The eigenvalue plot for a 50 meter per second flight speed at approximately 2 degrees angle of attack.

velocity ranging from zero to 50 meters per second can be seen in Figure 3.4.

The phugoid mode has positive eigenvalues at low speed demonstrating a loss of aerodynamic stability in the lower velocity range of transition. This instability supports the choice of pure thrust based lift during the transition stage of control. At the flight velocity of 50

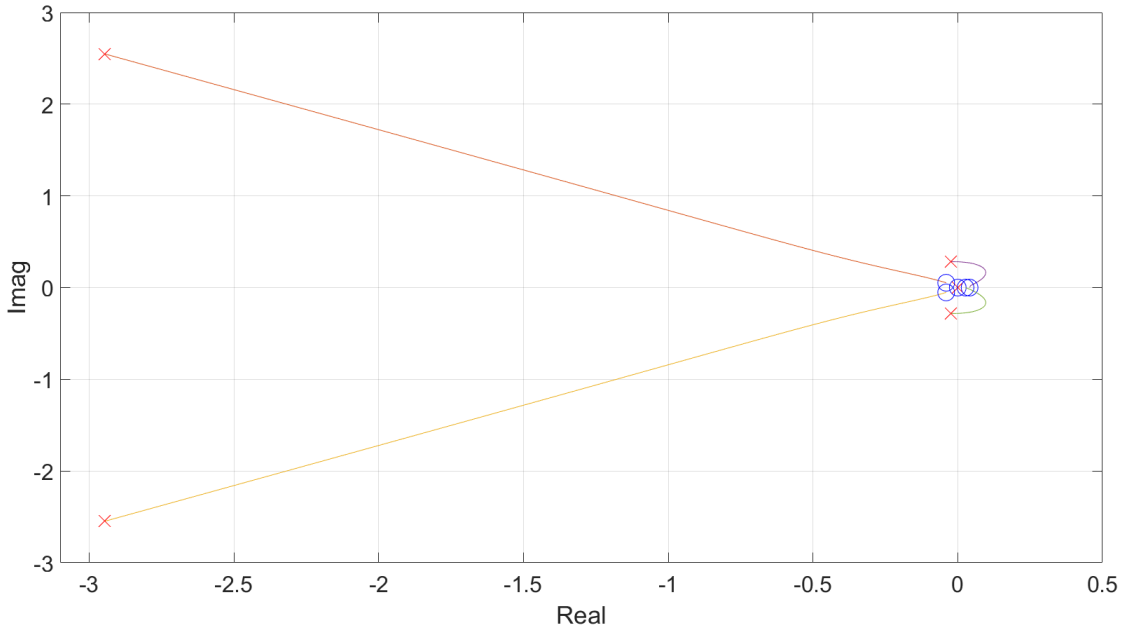

Figure 3.4: Eigenvalues resulting form a sweep of zero to 50 meters per second flight velocity.

meters per second, the system is stable without control. The stability is purely the rejection of disturbances and requires a controller for a desired state to be achieved.

To achieve a desired altitude and state equilibrium the use of a classical autopilot feedback design will be applied. The application for an altitude hold command via the classical method is to create a nested feedback loop [30]. The inner loop describes a θ controller and the outer loop describes the altitude controller. A high level block diagram can be seen in Figure 3.5.

A stable feedback controller is created for both θ and altitude loops. At the forward flight stage of transition, the only input that is considered available for control is the elevator. Having only one input reduces the system to a SIMO system. The controller can thus be designed purely by looking at feedback control for each loop as though the system was SISO

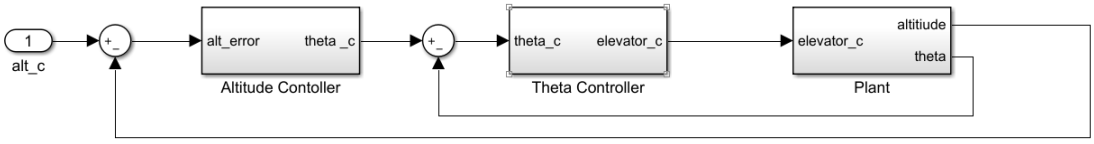

Figure 3.5: A nested loop block diagram depicting a high level altitude controller.

while including any previously made controller witnin the loop. Usage of PID controllers as means for theta and altitude control has been discussed as a plausible control design[34]. Applying PID controllers and tuning them results in PID gains

$$Altitude \quad PID \quad Gains = \begin{bmatrix} P \\ I \\ D \end{bmatrix} = \begin{bmatrix} 0.06 \\ 0.02 \\ 0.023 \end{bmatrix} \tag{3.32}$$

and

$$\theta \quad PID \quad Gains = \begin{bmatrix} P \\ I \\ D \end{bmatrix} = \begin{bmatrix} -0.39 \\ -0.2 \\ -0.18 \end{bmatrix}. \tag{3.33}$$

The determined PID gains are not excessively large and the controller effort is expected within limitations on the non-linear system. An example step command shows altitude tracking controller performance in Figures 3.6 and 3.7. The forward flight controller meets the controller goals. Altitude is held constant and stable. The steady altitude flight results in theta, alpha (and thus w, u, and q) all being constant and thus stabilized. The scheduled inputs are theoretically stabilized by the presence of the integrator of the PID. Non-linear simulation results are seen in the results section.

3.7 Transition Between Controllers

The controllers synthesized by the above methods all are expected to achieve the requirements of their respective regime. In this thesis the controllers will be left distinct and use

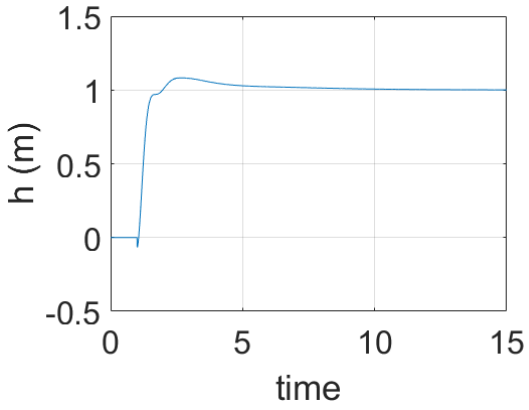

Figure 3.6: Altitude response due to altitude step command.

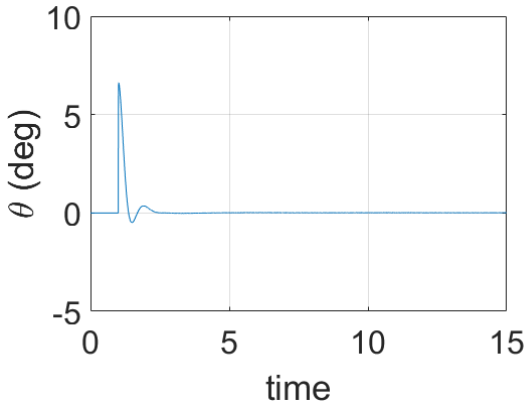

Figure 3.7: Theta response due to altitude step command.

of logic switches will be applied to merge them. The transition methods and their switching stages can be seen described below.

3.7.1 Forward Transition

Forward Transition: Hover To Transition Controllers

Forward transition begins with the VTOL controller commanded to maintain a hover equilibrium. The logic switch for hover to transition controllers checks u, w, and $\dot{w}$ and determines if the states are all be below chosen a threshold ϵ. This logic decision means that the switch will only occur when the translation is approximately zero and the change in velocity has settled to an approximate steady state value. Theta is unchecked as a non-zero theta will intuitively cause a non-zero 'u', and is thus a repetitive check.

Once the conditions are met switching of the controller then occurs. A memory hold function is applied at the moment of switching. The prior hover inputs are then given as initial feed forward inputs of the transition controller. The constant input, via memory hold,

lends a continuity between inputs as the switch occurs. In addition, any "learned" equilibrium inputs from the original hover controller are passed on to the transition controller. Saving learned equilibrium in memory removes unnecessary perturbation of initializing a new controller between switches. At the end of the switch, hover is maintained by the transition controller for a short period of time before the transition controller begins its scheduled events.

Forward Transition: Transition to Forward Flight Controller

Starting from a rotor tilt of 90 degrees the tilt is linearly decreased until the tilt is 70 degrees. Weight based thrust allows for a small tilt to largely increase the forward velocity of the system. Throughout the linear decrease, the feed forward input change as a function of tilt angle. The feed forward inputs maintain a constant altitude with zero vertical velocity when combined with the transition feedback control.

The 20 degree deflection from vertical tilt held until the flight velocity in forward flight becomes greater than 50 meters per second. At this speed the hybrid craft is within an aerodynamic stable region and transition between the transition and forward controllers will occur in a passively stable region.

Forward Transition: Forward Transition to Steady Level

Once 50 meters per second is reached, a switch is triggered the tail propeller then turns off and all feedback dependent control is shifted to the elevator. The elevator then momentarily stabilizes the vehicle until the forward flight scheduled events begin.

Following the switch of the vehicle to the forward flight controller, the elevator maintains altitude by creating an angle of attack through which aerodynamic lift can be applied to

the system. The thrust of the forward propellers is then linearly decreased from the weight based feed forward of transition down to a thrust level that can maintain the forward flight speed against drag. The given conceptual vehicle requires approximately 60 N of forward thrust at the 70 degrees rotor tilt angle to overcome drag.

The rotor then begins to decrease linearly again until a zero degree tilt is reached. During the tilt decrease, forward thrust, equivalent to drag at 50 m/s, is fed forward as a function of tilt. A forward thrust of approximately 24 N is the required thrust to overcome drag at zero rotor angle and velocity. During all scheduled events the elevator maintains the required altitude hold control goal and is the only feedback control input.

Once zero degrees is achieved the vehicle is in steady level flight and forward transition has been successfully completed. A switch can be applied to various other flight controller at this point as well.

3.7.2 Backward Transition

Backward Transition: Steady Level Flight to Transition Controller

Backward transition begins from the zero degree tilt and 24 N forward thrust condition. The signal for the backward transition switch comes from a pilot or a trajectory planning program. The steps for forward transition to steady level flight are then applied in reverse. The rotor tilt angle increases to 70 degree with the forward thrust feed forward control adjusting as a function of tilt. At 70 degree rotor tilt, the thrust then increases back to the previous, weight based, forward thrust. The elevator controls the system to maintain a constant altitude during these schedules.

For a short period before the next switch, the forward speed increase due to the config-

uration applying more than the required thrust to meet drag. The elevator then switches to a zero deflection and the tail propeller increases its thrust to weight match the weight ad counter torque needs of transition. The thrust inputs then maintain a short hold at the given altitude and tilt orientation. The rotor tilt then linearly increase to 92 degrees from 70 degrees and the vehicle begins to slow due to drag and backward propulsion.

Backward Transition: Transition Controller to Hover

Once near zero velocity has been achieved, the switch from transition to hover controller occurs. The controller starting from the 92 degree tilt switched immediately to vertical orientation of 90 degrees. The hard switch of the tilt is intended to avoid any unnecessary braking. The VTOL controller then stabilizes the system and ensures that any forward velocity is controlled to zero. Once equilibrium is reached the hover command is held. At this point a climb or decent command can be issued.

Chapter 4

RESULTS

In the following section, simulation of each control stage will be discussed as it pertains to the overall flight. Simulations will occur and the state and input information will be made available to the reader. Discussion of the states, the inputs, and the overall controller effectiveness will be discussed. For simulation in this thesis, the system will be simulated without a floor, i.e. altitude can decrease below zero.

As a note, mass and cg variation will be discussed for the hover condition only. The passing of equilibrium inputs from hover to transition results in less differentiation of state and input responses for the transition and forward flight. Discussion for the unloaded case and loaded case are very similar in nature, and thus the discussion will follow the unloaded case to avoid redundancy. A total flight of the unloaded and loaded cases will be shown at the end of the results and comments concerning their differentiation will be discussed at that time.

4.1 VTOL Controller: Hover Mode

4.1.1 Unloaded and No CG Variation

States: Unloaded and No CG Variation

The states of the tri-copter using the VTOL controller with a desired hover equilibrium can be seen in Figure 4.1.

Forward Velocity(u): The forward velocity can be seen to start from 0 and increase slightly

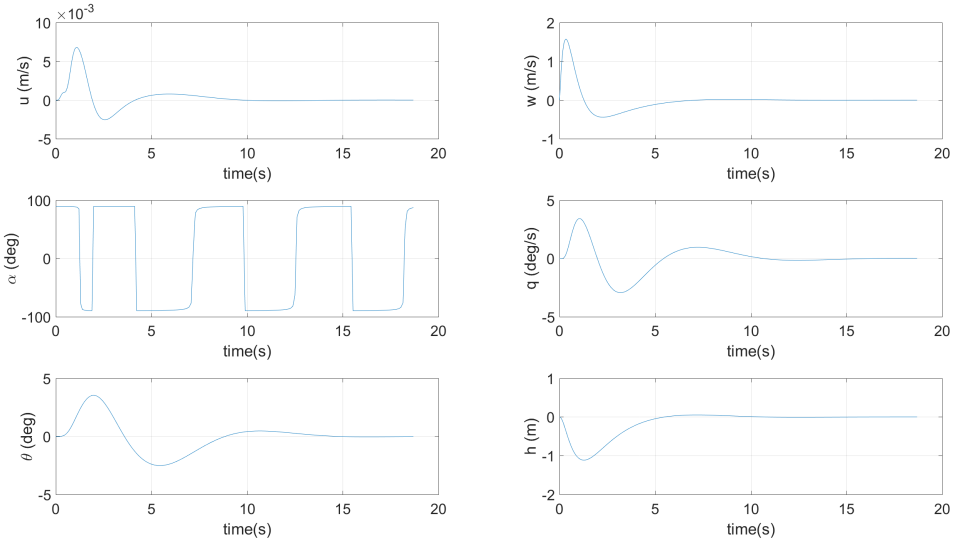

Figure 4.1: Stated of hybrid vehicle in hover mode with 0 Kg added payload and 0 m variation of the CG.

due to deflection of the forward propeller tilt. The velocity quickly returns to zero. The forward velocity is also seen to have a very small magnitude compared to the other states.

Vertical Velocity (w): The vertical velocity accelerates due to gravity before the thrust reaches weight values. The thrust then increases and reduces the magnitude of vertical velocity to zero.

Angle of Attack(α): Meaningless at low forward velocity. This state will be removed from discussion until transition to forward flight.

Pitch Rate(q): There is a small fluctuation in pith rate as the aerodynamic moment induced by vertical velocity causes net torque. The effect of pitch rate is seen through theta. This state will not be discussed during the remainder of the paper.

Euler Angle(θ):The increase in vertical velocity due to gravity creates a pitching up moment due aerodynamic drag. The forward wing has a larger drag resulting in the pitch direction being positive. The aero induced moment causes theta to increase to approximately two

degrees before the VTOL controller brings it to a steady zero degrees.

Altitude (h): Altitude is decreased due to gravity. Once inputs achieve weight based values the altitude levels out and becomes constant.

Inputs: Unloaded with No CG Variation

The inputs of the tri-copter using the VTOL controller with a desired hover equilibrium can be seen in Figure 4.2.

Forward Thrust ($\mathbf{T_p}$): Forward thrust begins at zero then overshoots its equilibrium be-

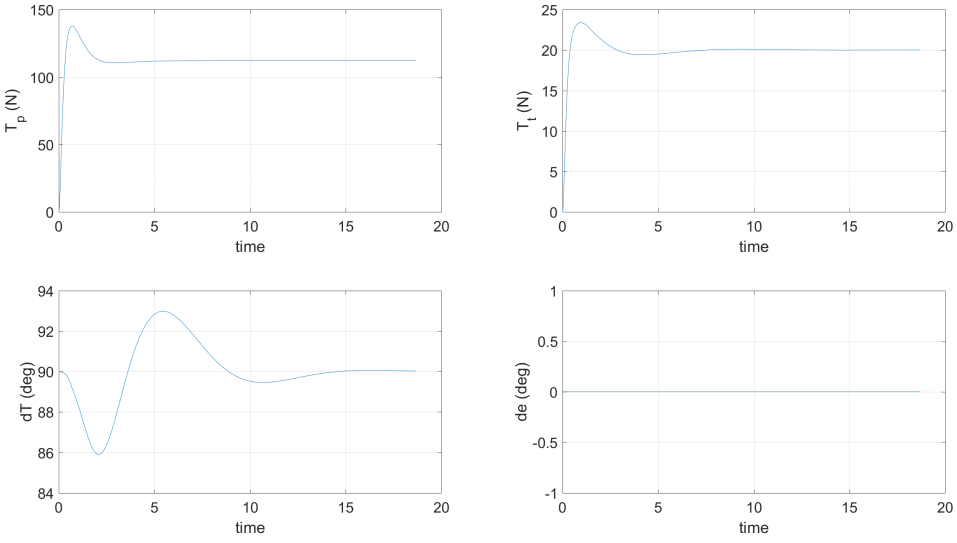

Figure 4.2: Inputs of hybrid vehicle in hover mode with 0 Kg added payload and 0 variation of the CG.

fore settling down to its final input value for the hover condition. This value is approximately 112 N.

Tail Thrust ($\mathbf{T_t}$): Tail thrust begins at zero then overshoots its equilibrium before settling down to its final input value for the hover condition. This value is approximate 20 N.

Rotor Tilt (dT): Starting from 90 degrees (vertical) the tilt only deviates about three degrees. The variation is due to coupled inputs being used to achieve equilibrium, followed by control of the non-zero surge velocity to zero.

Elevator Deflection (de): Elevator is not applied in VTOL control and will be removed from discussion until the forward flight section.

Discussion: Unloaded with no CG Variation

The VTOL controller demonstrates a stabilization of the states u, w, theta, q, and altitude, seen in Figure 4.1, by the input process, seen in Figure 4.2,with no payload and no variation of the center of gravity. As the system initiates, all states begin at zero and an expected drop in altitude occurs as the thrust inputs initiate. In reality the ground would prevent this drop and a slow start up would guarantee that the vehicle remain on the ground as it learns the equilibrium input values. The inputs all remain within reasonable ranges. Thrust is within the specified limits and the tilt angle is small. The system is acting as expected and achieves the controller goals set forth in the VTOL control strategy for hover mode.

4.1.2 Loaded with No CG variation

States: Loaded with No CG variation

The states of the tri-copter using the VTOL controller with a desired hover equilibrium can be seen in Figure 4.3 with varied kilograms of added mass.

Forward Velocity (u): The magnitude of forward velocity deviation from zero increases as a higher mass is applied. This deviation is due to the increased vertical velocity creating a larger aerodynamic pitching moment that in turn allows more gravitational effects to be felt on the forward body axis. The time to settle to equilibrium is also increased.

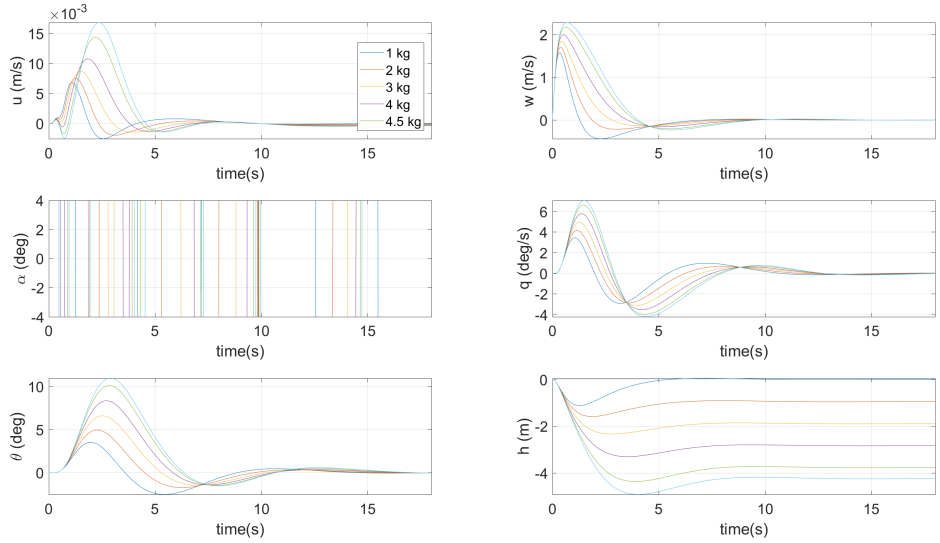

Figure 4.3: State of hybrid vehicle in hover mode starting with 0-4.5 kg added payload and 0 m variation of the CG.

Vertical Velocity (w): The vertical velocity increases in magnitude and settling time with increased gravitational force compared to the unloaded model.

Euler Angle(θ): The higher vertical velocity causes a higher pitch moment that then results in a higher theta deviation. Theta deviation increases to approximately ten degrees at full loading.

Altitude (h): The effect of gravity can be seen to cause increased loss of altitude due to the presence of increase mass.

Inputs of Loaded with No CG variation

The states of the tri-copter using the VTOL controller with a desired hover equilibrium can be seen in Figure 4.4 with varied kilograms of added mass.

Forward Thrust ($\mathbf{T_p}$): The equilibrium values can be seen to increase with increased mass.

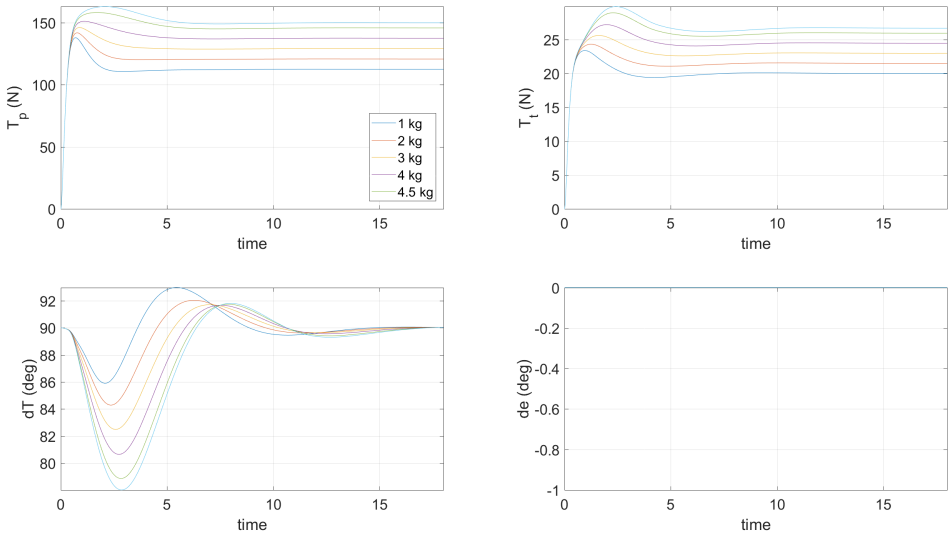

Figure 4.4: Inputs of hybrid vehicle in hover mode starting with 0-4.5 kg added payload and 0 m variation of the CG.

Tail Thrust ($\mathbf{T_t}$): The equilibrium values can be seen to increase with increased mass.
Rotor Tilt (dT): The increased mass causes a larger variation of the tilt angle. The larger deviation is the result of higher state deviation above and coupled inputs. The rotor tilt angle begins to approach 75 degrees.

Controller Effectiveness of Loaded Hybrid Vehicle with No CG Variation

The states of the tri-copter using the VTOL controller with a desired hover equilibrium and added mass can be seen in Figures 4.3 and 4.4. As added mass increases the responses and extends the time to settling. The inputs and states share a similar effect scaling in size and transient time. New equilibrium values are found for both the thrust inputs. Regardless of mass, the added the system remains stable and the inputs remain reasonable. The controller remains effective in the simulation of increased payload.

4.1.3 Unloaded with CG Variation

States: Unloaded with CG Variation

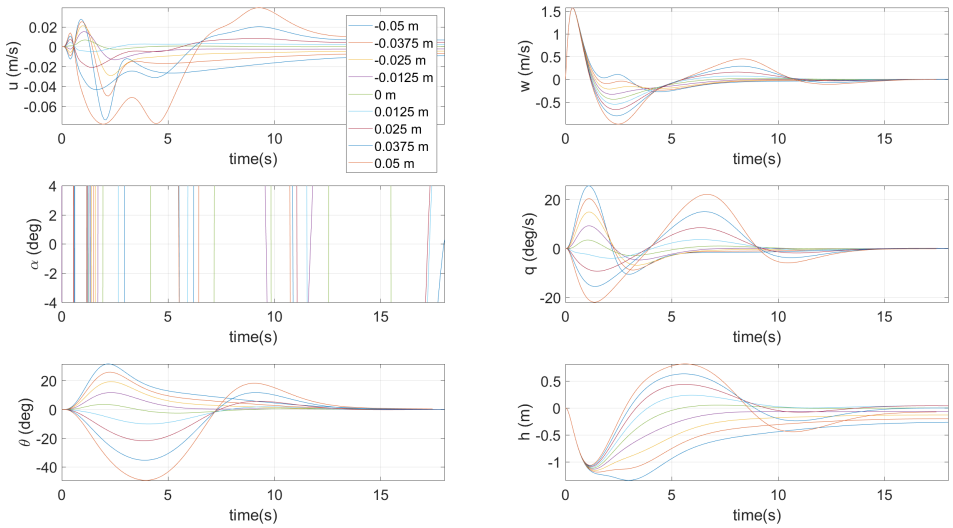

Figure 4.5: State of hybrid vehicle in hover mode starting with 0 kg added payload and -0.05 to 0.05 m variation of the CG.

The states of the tri-copter using the VTOL controller with a desired hover equilibrium and -0.05 to 0.05 m variation of the CG can be seen in Figure 4.5.

Forward Velocity (u): The forward velocity is an order of magnitude larger than the non-deviation case. The result of a largely increased theta angle. Movement of the CG forward creates larger perturbations and settling time of forward velocity. The velocity is bounded but values maintain small non-zero values. These values slowly disappear as the rotor tilt settles to vertical.

Vertical Velocity (w): The vertical velocity has higher values as well as alternating between positive and negative values with CG variation. The variation is due to the equilibrium

input feed forward being incorrect for the given moment arms. Movement of the CG forward acts to increase the overshoot in the negative direction as well an extended settling time. The backward motion of the CG settles similarly to the unloaded case. Both directions of CG variation change the moment arm between the thrust points and the CG acting to lower performance of the base control model.

Euler Angle(θ): The theta angle increase to positive 25 degrees with a backward motion of the CG and decreases to -50 degrees as the CG is adjusted forward. The increase is due to adjusted moment arms of the thrust inputs due to CG variation. The magnitude is the result of the control input sensitivity increasing based on cg variation.

Altitude (h): Altitude values show an increase in altitude with forward CG movement. The backward CG movement induces a larger loss of altitude. These gains and losses correspond to the combination of theta and w variations discussed above.

Inputs of Unloaded and CG Variation

The states of the tri-copter using the VTOL controller with a desired hover equilibrium can be seen in Figure 4.6 with -0.05 to 0.05 m variation of the CG.

Forward Thrust ($\mathbf{T_p}$): The equilibrium input of the forward thrust differ by about 10 N from a 0 CG variation position. The variation is due to the new moment arm. Fluctuations also increase in time length and the integrator gains adjust to the new CG position.

Tail Thrust ($\mathbf{T_t}$): The equilibrium input of the tail thrust differ by about 10 N from a 0 m CG variation position. The variation is due to the new moment arm.

Rotor Tilt (dT): The variation of the rotor tilt angle now increases to large magnitudes. The limit of 180 degrees (which would then the put the proportional controller into a spin) is not reached . Variation is much larger than the base configuration with fluctuations of 50-60 degrees about vertical. The settling time is also much slower to integrate to vertical tilt.

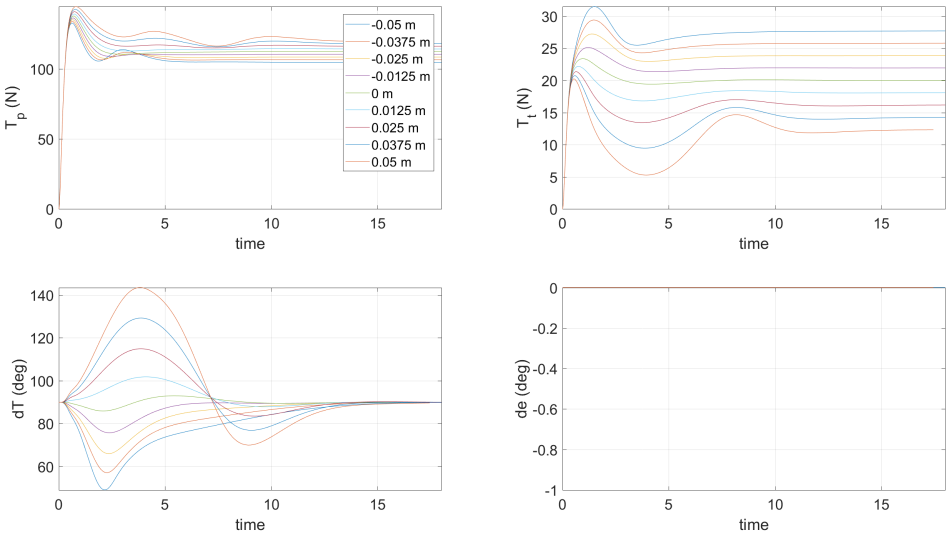

Figure 4.6: Inputs of hybrid vehicle in hover mode starting with 0 kg added payload and -0.05 to 0.05 m variation of the CG.

Controller Effectiveness of Unloaded and CG Variation

Figures 4.5 and 4.6 represents an unloaded case with deviation in center of gravity. The stability of the states holds with the increased magnitude of the states due to the CG variation, approximately 15 percent of the chord. The vertical velocity begins to show a poorer stabilization performance affecting the altitude in turn. In general movement of the center of gravity toward the nose of the hybrid craft appears to alter the controller performance in a more negative fashion than positive cg variation. This poorer stability is due in large part to the tail propeller having an increased pitch effect with a now overly high initial equilibrium feed forward. The difference is integrated but the initial error has a more aggressive effect with forward cg variation than backward variation.

The inputs begin to deviate from their equilibrium values largely to adjust for the center of gravity adjustment. The rotor tilt angle begins to deviate from vertical to approximately

50 degrees before settling. The most notable changes occur in the thrust levels of the hybrid craft. The adjustment of the moment arm of the thrust inputs require the integrator to find a steady state value as opposed to the feed forward inputs meeting this need. The controller begins to reach extremes of tilt but it remains within a plausible input and stabilizes the system still. The forward velocity is now non-zero but bounded and slowly approaching zero as the tilt reaches vertical. The achievement of equilibrium is the result of the VTOL controller meeting the majority its requirement goals. The performance is poorer compared to the base model but still successful.

4.1.4 Loaded with CG Variation

States: Loaded and CG Variation

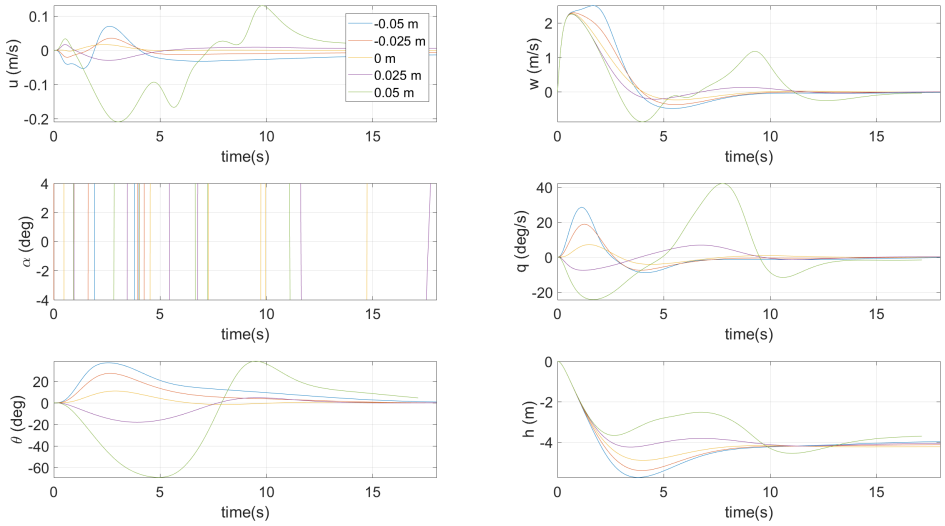

Figure 4.7: State of hybrid vehicle in hover mode with 4.5 kg added payload and -0.05 to 0.05 m variation of the CG.

The states of the tri-copter using the VTOL controller with a desired hover equilibrium

and with 4.5 kilograms added mass and CG variation can be seen in Figure 4.7.

Forward Velocity (u): The majority of forward velocities are clustered with the forward CG variation of 0.5 meters demonstrating an unsteady trajectory towards equilibrium. The effect of CG variation is increased due to mass. The forward velocities are small non-zero values but all velocities remain bounded and approach zero as tilt approaches vertical.

Vertical Velocity (w): The vertical velocity is similar to its unloaded with CG variation case. There is an increase in magnitude with larger variation in the forward direction. There is both positive and negative velocities apparent as the CG varies. All values settle to zero.

Euler Angle(θ): The theta angle has large deflections at the CG variation extremes. The effect has been magnified by increased weight. The values remain below a magnitude of 90 degrees but show poorer performance.

Altitude (h): The altitude is decreased due to the added mass creating an increased vertical velocity. Settling time is increases and largest deflection occur. These variations are worse with forward CG variation.

Inputs: Loaded and CG Variation

The inputs of the tri-copter using the VTOL controller with a desired hover equilibrium can be seen in Figure 4.8 with 4.5 kilograms of added mass and 0.05 meters of CG variation.

Forward Thrust ($\mathbf{T_p}$): The transience in settling time is increased as the CG is moved forward. Backward motion of the CG variation performs similarly to no CG variation. The equilibrium value has increased from the non-loaded case.

Tail Thrust ($\mathbf{T_t}$): Higher fluctuations occur before equilibrium. An unsteady trajectory to equilibrium results from forward CG variation. The values of thrust approach negative thrust but achieve equilibrium in all cases.

Rotor Tilt (dT): The tilt angle approaches the limits of proportional control. Tilt angle remains within 180 but are largely past linear assumptions. The worst effect is seen with forward CG variation but the backward CG variation shows decreased performance with

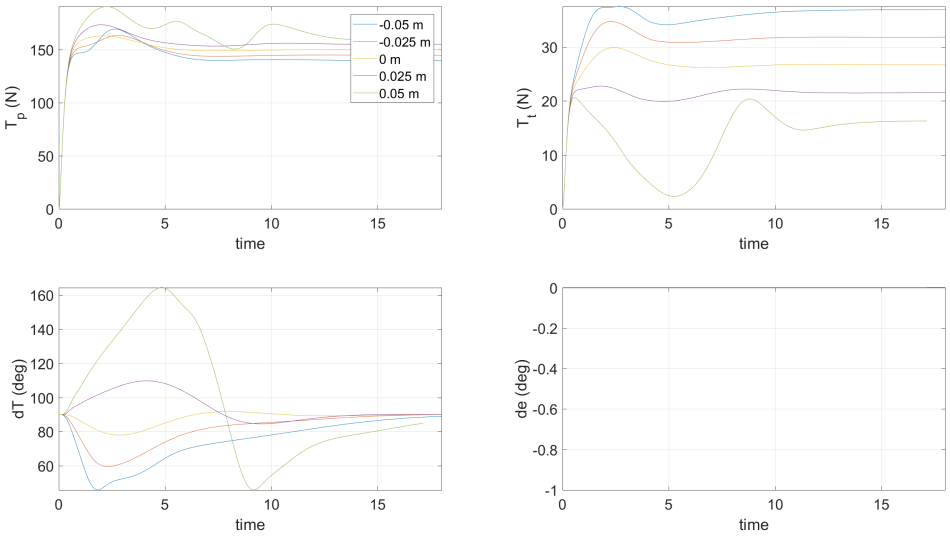

Figure 4.8: Inputs of hybrid vehicle in hover mode starting with 4.5 kg added payload and -0.05 to 0.05 m variation of the CG.

added mass as well. The integration to vertical tilt is slower with adjusted cg variation.

Controller Effectiveness of Loaded and CG Variation

The final Figures for hover simulation are seen in 4.8 and 4.7. The entirely loaded cases and CG varied cases are extreme but still stabilized. The amount of time necessary to settle are much larger than the unloaded model. The theta angles and tilt angels begin to push input limits but remain within the plausible domain. The inputs are similar to the CG variation case with larger magnitude and settling time. The effect of added mass and CG variation leads to the poorest controller performance when variation is forward.

The VTOL controller maintains stability of the hover equilibrium. All states and inputs are bounded. Forward velocity is small and non-zero but remains bounded as the rotor tilt

approaches vertical. Going forward the learned equilibrium will allow the transition controller to avoid large initialization deviations. The goals for VTOL are still successfully met.

4.2 VTOL Controller Climbing/Descending

4.2.1 VTOL Controller: Climbing

States: Climbing

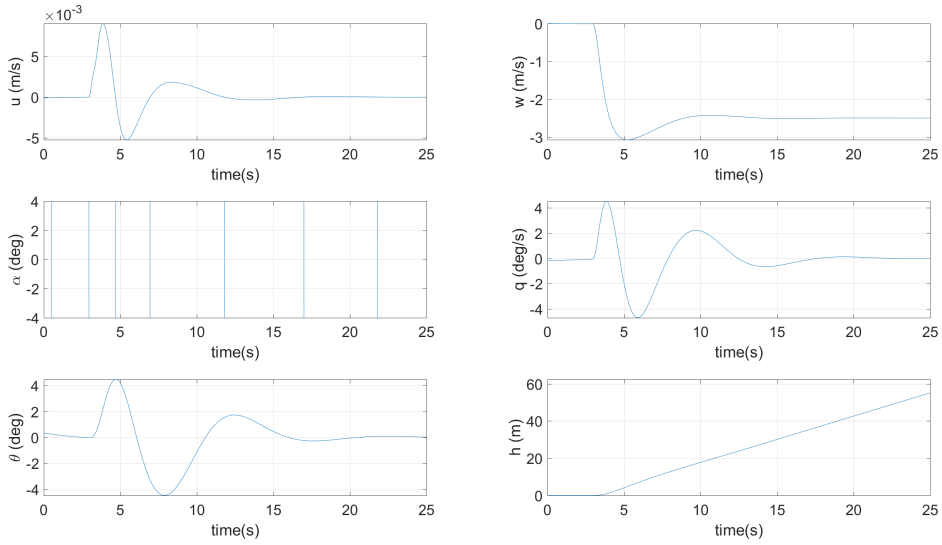

Figure 4.9: State of hybrid vehicle with 2.5 meter per second climb starting from hover achieved with hover mode and climbing with 0 kg added payload and 0 m variation of the CG.

The states of the tri-copter using the VTOL controller starting from hover starting with 0 kg added payload and 0 m variation of the CG can be seen in Figure 4.9.

Forward Velocity (u): The forward velocity fluctuates slightly as transition begins at approximately 3 seconds. The magnitude is small and reaches equilibrium.

Vertical Velocity (w): The demanded velocity of 2.5 meters per second is achieved and held with slight overshoot.

Euler Angle(θ): The theta angle can be seen to fluctuate between positive and negative five degrees as the climb begins. This fluctuation is due to a change in aerodynamic moment due to vertical velocity induced drag and drag moment. The inputs stabilize about the desired velocity.

Altitude (h): The altitude increases linearly as the vertical velocity is held.

Inputs Climbing

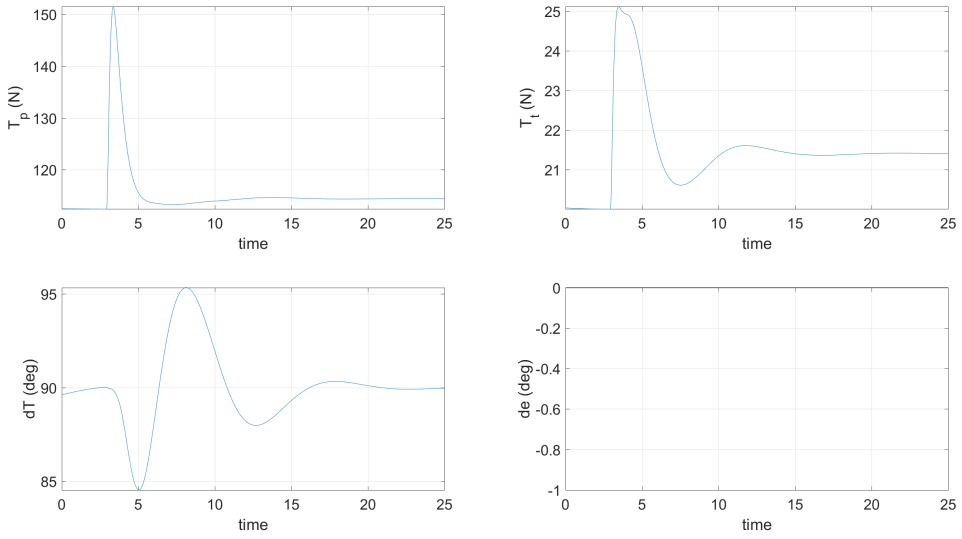

Figure 4.10: Inputs of hybrid vehicle with 2.5 meter per second climb starting from hover.

The inputs of the tri-copter using the VTOL controller starting from hover and climbing with 0 kg added payload and 0 m variation of the CG can be seen in Figure 4.10.

Forward Thrust ($\mathbf{T_p}$): There is a pulse as increased lift is generated to create due to proportional error caussed by the 2.5 meter per second command. It achieves equilibrium

shortly after. The final input is increased slightly from its initial position. The increase is due to the presence of aerodynamic drag and moment. There is also an associated increase with the rotor defection to maintain equilibrium.

Tail Thrust ($\mathbf{T_t}$): Similarly the tail thrust has a pulse as vertical velocity is increased before settling down to a steady value slightly above its initial value. The increase is due proportional control effort causing an initial upward pitch.

Rotor Tilt (dT): There is slight fluctuation in the tilt angle to adjust the forward velocity back to zero following a non-zero theta induced acceleration caused by the pitching moment. It remains within a seven degrees of vertical.

Controller Effectiveness of Climbing

Figures 4.9 and 4.10 represent the hybrid vehicle dynamics during climb. The assumption that vertical climbing occurs following a hover equilibrium is made. Reaching equilibrium is not necessary for the unloaded model but loading and CG variation will make use of learned equilibrium states from hover to allow a gentle transition. Hover mode will be the starting point for either climb or descent. The states remain stable and follow the command. From the hover equilibrium, climb begins and a constant increase in altitude is achieved. The theta angle has a small fluctuation between plus and minus five degrees and is acceptable. The inputs spikes as climb mode is entered but reach steady state without exceeding their limitations. The change in the tilt of this thrust also remains within a bounds of about seven degrees deflection from its vertical position and is acceptable. The climb of the vehicle is achieved and stability is maintained. The VTOL control goals for vertical velocity climb are met.

4.2.2 VTOL Controller Descending

States Descent

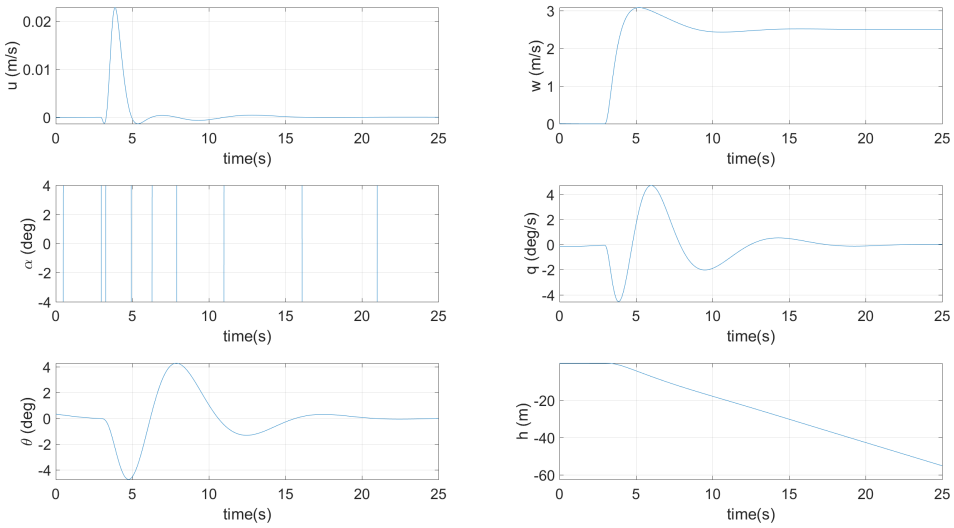

Figure 4.11: State of hybrid vehicle with 2.5 meter per second descent starting from hover

The states of the tri-copter using the VTOL controller starting from hover and descending can be seen in Figure 4.11.

Inputs Descent

Controller Effectiveness of Descending

A reflected change of the states and inputs of the descent command as compared to the vertical climb can be seen in Figures 4.11 and 4.12. The velocity command is achieved and stable as noted by the w velocity. The altitude can be seen to decrease linearly as demanded. All other states remain in reasonable domains with small magnitudes and transience. The inputs of thrust can be seen to drop and hold equilibrium at lower than hover values. The decrease is expected as gravitational force assists in achieving the vertical descent. The tilt

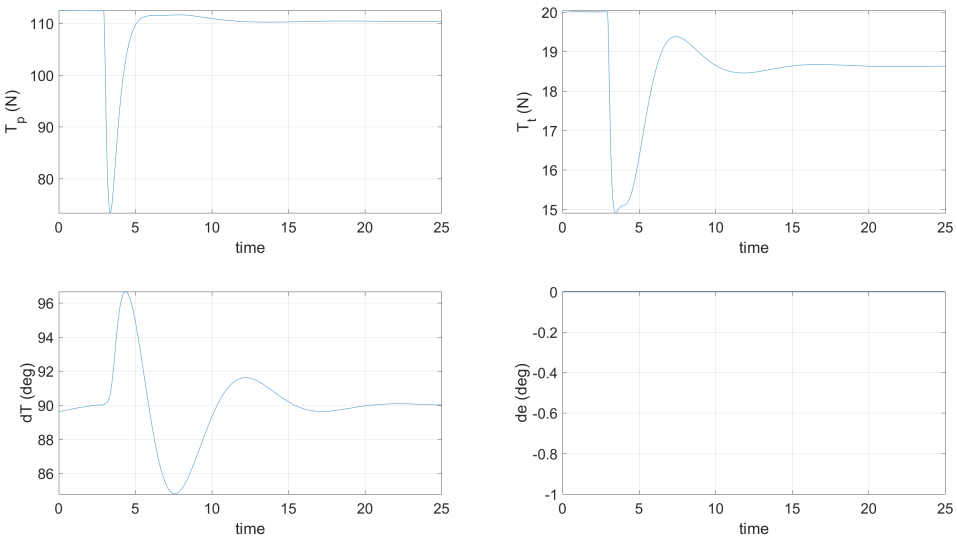

Figure 4.12: Inputs of hybrid vehicle with 2.5 meter per second descent starting from hover.

angle has small deviation from vertical and achieves it vertical equilibrium over time. All inputs are stable and reasonable. For the base conceptual model the VTOL controller goals are met for descent.

4.3 Forward Transition

The dynamic responses of the transition controller will now be simulated and discussed. All simulations going forward assume that hover is achieved and that transition occurs at the altitude of hover equilibrium.

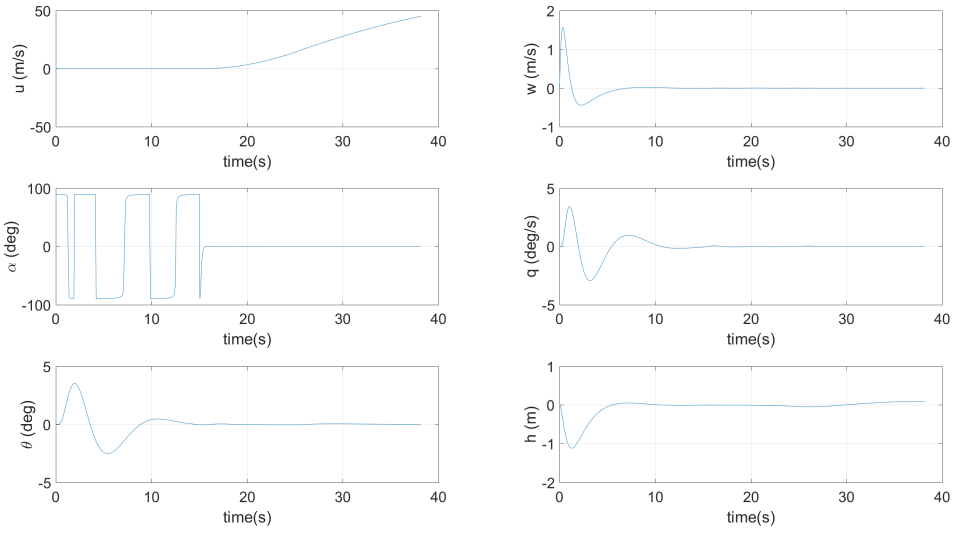

Figure 4.13: States of hybrid vehicle during forward transition.

4.3.1 Hover to Forward Transition

States of Hover to Forward Transition

The transition dynamics can be seen in 4.13.

Forward Velocity (u): The forward velocity increases as the tilt schedule begins at approximately 15 second. The thrust being applied along the tilt direction overcomes forward drag resulting in velocity increase. The effect drag can be seen by the concave down nature of the curve. Forward acceleration magnitude is decreasing with increased velocity as aerodynamic drag grows.

Vertical Velocity (w): The vertical velocity maintains a value of zero following VTOL hover command. The value remains at zero with only slight pertubations due to imperfect thrust values. The vertical velocity also corresponds to the desired angle of attack of zero.

Angle of Attack(α): The angle of attack following transition achieves a steady value of zero. Compared to pre-transition data, the forward velocity is now at a speed where angle of

attack is applicable. The effect of forward velocity can be seen at approximately 15 seconds. The curvature approaches zero suggesting that the w to u ratio is decreasing with forward velocity.

Euler Angle(θ): Theta remains zero during transition due to control effort and shows only small variation due to imperfect thrust values being controlled to equilibrium.

Altitude (h): The altitude remains approximately constant during transition. Only slight changes due vertical velocity and theta movement.

Inputs of Hover to Forward Transition

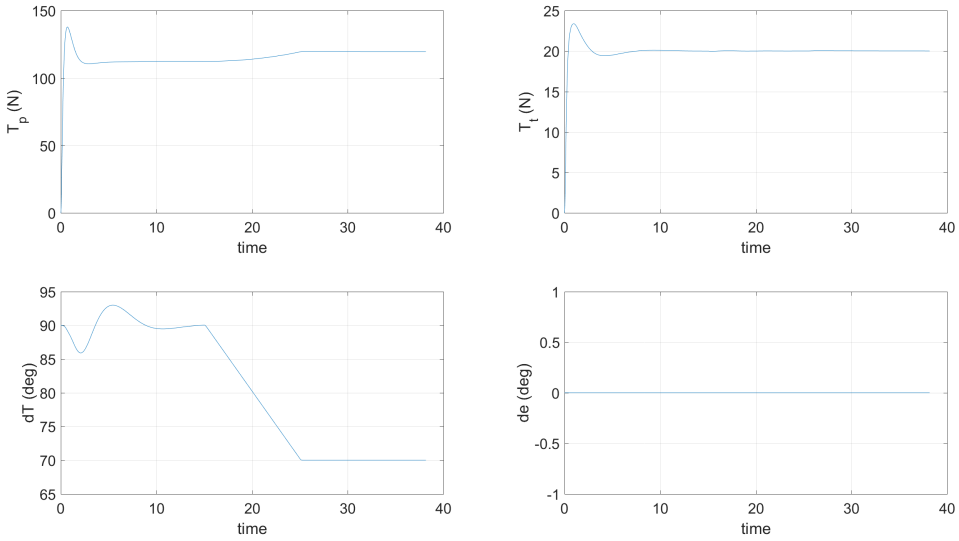

Figure 4.14: Inputs of hybrid vehicle during forward transition.

The transition inputs can be seen in 4.14.

Forward Thrust ($\mathbf{T_p}$): The initial equilibrium is held then increased as a function of tilt angle. The value doesn't fluctuate as it is scheduled.

Tail Thrust ($\mathbf{T_t}$): The tail thrust remains approximately constant as no additional thrust

is required to maintain pitch orientation. There is small fluctuation as the tilt occurs.
Rotor Tilt (dT): The rotor tilt can be seen to decrease in value linearly. The decrease is scheduled and stops decreasing at 70 degrees.

Controller Effectiveness of Hover to Transition

The control strategy section described above makes use of a memory hold during the switch of the transition controller. Starting from the hover condition, equilibrium inputs are passed forward to to the feed forward portion of the transition controller and can be seen by the smooth transition. The switch of controllers occurs after settling of equilibrium is approximately achieved as discussed in the switching controllers section.

The forward transition was activated at about 15 seconds. The tilt begins its scheduled maneuver once switching occurs. Thrust inputs follow a feed forward that is a function of tilt angle to maintain pitch orientation during transition. The effects of forward transition at about 15 seconds when the surge velocity begins to increase. All other states remain at relatively zero as is desired. No disturbances are assumed and there is little fluctuation once the equilibrium is passed from hover to the transition controller.

All states remain stable, the inputs remain constant and within their limits following the 70 degree tilt change, and the velocity is increasing as desired. The transition controller goals are met on the non-linear system.

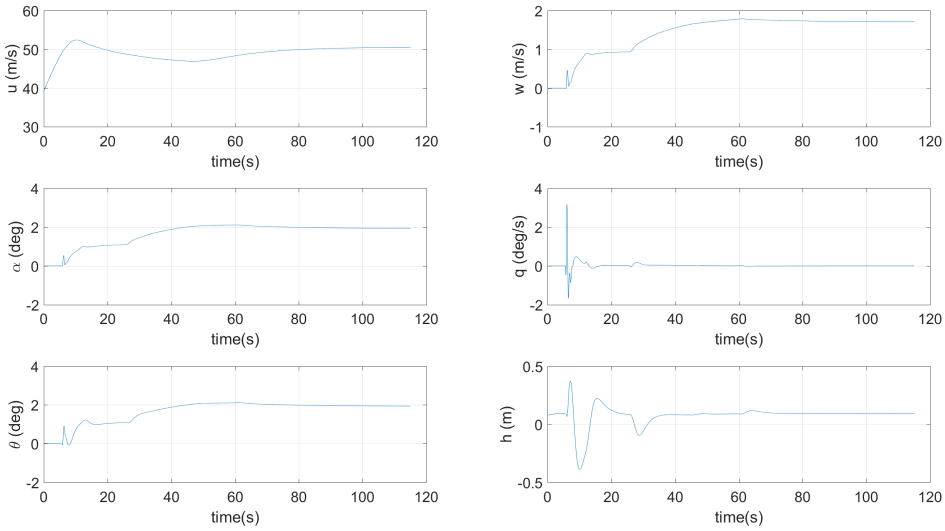

Figure 4.15: States of hybrid vehicle during transition to forward flight.

4.3.2 Transition to Forward Flight

States: Transition to Forward

The states of the switch to forward flight mode from transition are seen in 4.15.

Forward Velocity (u): The forward velocity can be seen to increase to 50 meters per second. Once 50 meters is achieved, the speed then decreases slightly due to the presence of lift induced drag (from the now applied elevator) and the scheduled thrust levels. It reaches an equilibrium speed of approximately 50 meters per second after all scheduled inputs have terminated.

Vertical Velocity (w): The vertical velocity can be seen to spike and then reach approximately one meter per second. The spike is due to the angle of attack created by elevator usage at the initial weight based thrust. The thrust then decreases, resulting in the one meter per second hold, it then grows to reach a constant velocity of about two meters per second. The constant nature of this speed is equivalent to a constant angle of attack. The

velocity is held once the scheduled inputs terminate.

Angle of Attack(α): The angle of attack is now a non-zero value. An initial perturbation occurs at seven seconds due to a zero elevator command overshooting the needed deflection. Next it increases as the thrust decreases on its schedule. The increase is a result of more aerodynamic lift being required to maintain altitude. The trajectory follows the same trajectory as vertical velocity. Angle of attack is function of the ratio of vertical velocity to forward velocity so this makes sense.

Euler Angle(θ): The theta angle follows the angle of attack trajectory and remains constant after reaching an approximate value of two degrees. The similarity of the curve with the angle of attack implies steady level flight conditions are being met.

Altitude (h): There is a small fluctuation of altitude during the switch but overall altitude is maintained. There are three fluctuations of note. The large fluctuation due to the initial switch occurring at seven seconds and is due to the elevator inducing an angle of attack spike which induces aerodynamic lift that is more than that required for weight. The small fluctuation at 30 seconds is the result of the tilt schedule beginning. Finally, the perturbation at 65 seconds occurs when the final configuration (with zero tilt) is achieved and the schedule terminates. The time length of the largest fluctuation is approximately 10 seconds with magnitude around 0.8 meters peak to peak. The variation is slow and acceptable performance.

Inputs: Transition to Forward

The inputs of the switch to forward flight mode from transition are seen in 4.16.

Forward Thrust ($\mathbf{T_p}$): The forward thrust enters the previously described schedule. Thrust decreases to 60 N, then decreases as a function of tilt angle until it reaches 24 N at zero degrees tilt.

Tail Thrust ($\mathbf{T_t}$):The tail thrust is turned off once the switch to the forward flight controller is made at seven seconds.

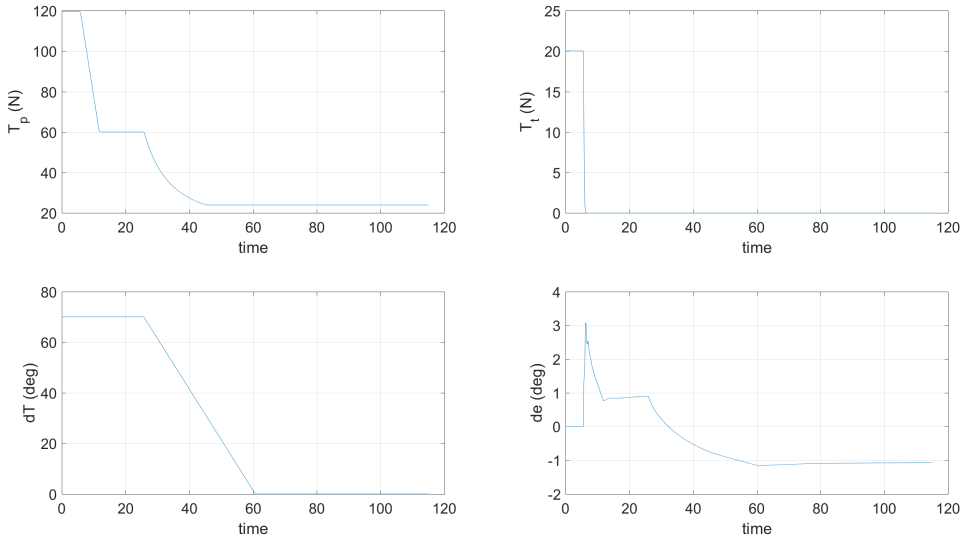

Figure 4.16: Inputs of hybrid vehicle during transition to forward flight.

Rotor Tilt (dT): Starting at 25 seconds the tilt begins to decrease from 70 degrees linearly to zero degree deflection.

Elevator Deflection (de): The elevator is applied immediately at the switch at seven seconds. There is an initial to counter the pitch created by a forward thrust input without counter tail thrust torque. There is a slight overshoot resulting in a slight fluctuation near the peak. It then decreases as to a steady value as the thrust decrease to steady level conditions with thrust at 60 N. The hold is maintained until 25 seconds when the tilt schedule begins. It then decreases its deflection as zero degree tilt is approached. The decrease is due to decreasing pitching moment created by the forward thrust.

Controller Effectiveness of Hover to Transition

The switch results in various shocks felt through states. The presence of aerodynamic lift and its induced drag effects are seen in u and w. The forward speed remains around

the flight velocity of forward controller design and reaches equilibrium at about this value following the termination of the input schedule.

The angle of attack remains positive and demonstrates that aerodynamic lift is being applied to the vehicle as well as thrust lift. Angle of attack adjusts to meet the lift requirements of the scheduled inputs. The theta values mimic the angle of attack values during this time. The similarity of these state is expected near a steady level flight condition. Angle of attack and theta are equal at a steady level flight condition. The data thus is adding validity to a steady level flight control effect, a desired result of the forward flight controller. The altitude varies by approximately 0.4 meters over a course of approximately 10 seconds. The fluctuation is small and the time span is large. The transient nature can then be considered an acceptable variation about the desired altitude.

The inputs, with the exception of the elevator, are all scheduled during this stage. The trajectories seen in Figures 4.15 and 4.16 demonstrate the effectiveness of the elevator to maintain stable dynamics during transition to the forward flight. Of note as well, there is a large drop in forward thrust compared to the required 120 N in hover mode. This thrust decrease is desired and results in a more efficient usage of thrust for flight compared to the weight based thrust.

The goals for the forward flight controller of maintaining altitude and stable states during the scheduled variation is achieved.

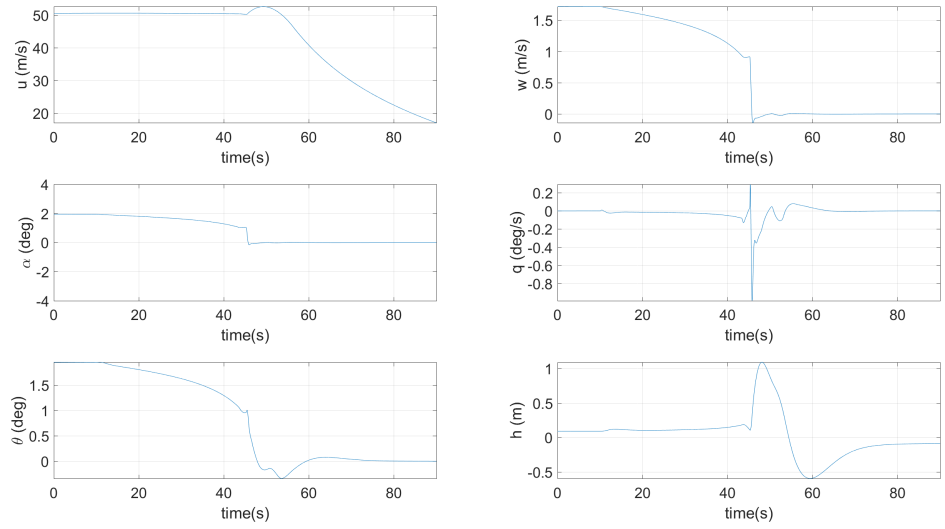

Figure 4.17: States of hybrid vehicle during backward flight transition.

4.4 Backward Transition

4.4.1 Switch form Forward to Transition Controllers

States: Forward flight to BWD Transition

The states of the switch to transition controller mode from forward flight are seen in 4.17.

Forward Velocity (u): The forward velocity remains constant at the steady level flight condition speed until the switch occurs. The weight based thrust is reached before the tilt angle returns to 90 degrees thus there is an accelerating force when the rotor tilt is at 20 degrees. The result is an increase in the forward velocity magnitude for a short period after 48 seconds. Once the tilt moves past the vertical orientation, forward velocity begins to slow due to drag and a slight amount of backward propulsion.

Vertical Velocity (w): The vertical velocity decreases as the tilt increase. The reverse of its previous transition. The decrease is due to the adjusted angle of attack needed to

maintain lift decreasing. The value quickly reaches zero once the tail thrust input begins.

Angle of Attack(α): The angle of attack decreases from its constant value as less lift is required. The trajectory mirrors the forward transition trajectory. The angle of attack reaches a zero equilibrium once the tail thrust starts. It reaches this value more quickly than theta.

Euler Angle(θ): Theta also decreases as less lift is needed and reaches the zero degree configuration as is desired by the transition controller. Theta decreases to zero less quickly than angle of attack. The result is that a non-zero theta exist for a short period with zero angle of attack.

Altitude (h): There is a fluctuation of altitude that occurs immediately following the switch. The increase occurs while theta is positive and angle of attack is zero. The forward velocity is applied at an angle of theta with no vertical velocity to cancel out the gain in altitude. The moment theta switches to a negative value the altitude begins to drop due to the same effect. Once theta reaches zero the altitude becomes constant.

Inputs: Forward flight to BWD Transition

The inputs of the switch to transition controller mode from forward flight are seen in 4.18.

Forward Thrust ($\mathbf{T_p}$): The forward thrust follows its pre-stated schedule. The thrust increases as function of rotor tilt until 70 degrees is achieved. The thrust then increases to its weight based value. Forward thrust overshoots for moment then settles to equilibrium.

Tail Thrust ($\mathbf{T_t}$): The tail thrust is activated at the moment of switching. It quickly climbs to the weight based value from transition. A small amount of overshoot is present and equilibrium is reached shortly thereafter.

Rotor Tilt (dT): The tilt angle is increased from 0 to 92 linearly as is scheduled. The extra 2 degrees back act as a brake to slow the vehicle more quickly.

Elevator Deflection (de): The elevator increase its deflection to create a counter torque created from the tilted and increasing thrust. The deflection trajectory mirrors the forward

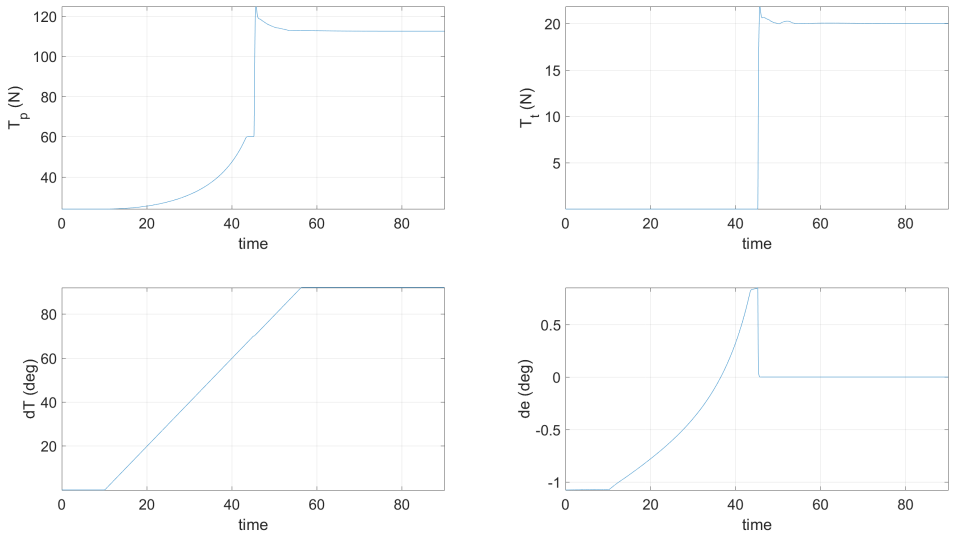

Figure 4.18: Inputs of hybrid vehicle during backward flight transition.

transition trajectory. The elevator then settles to zero following the switch to tail thrust.

Controller Effectiveness of Hover to Transition

Beginning from forward flight condition, seen as the initial value of the states in Figure 4.17, backward transition occurs. A majority of the inputs, seen in Figure 4.18 are scheduled during this time. The tilt of the rotors increasing signals the beginning of the switch. The states can be seen to function similarly to the forward transition. There is a lag in the controller as vertical velocity equivalent to zero is achieved before theta is zero. The lag results in a fluctuation of altitude. The variance of altitude occurs over 15 seconds and can be considered a gentle transience.

All states remain stable and all inputs are within the acceptable limits. The switch is successful with both the forward and transition controller goals being met.

4.4.2 Transition to Hover

States: Transition to Hover

The transition states can be seen in Figure 4.19.

Forward Velocity (u): Forward velocity decrease as a result of drag forces and slight re-

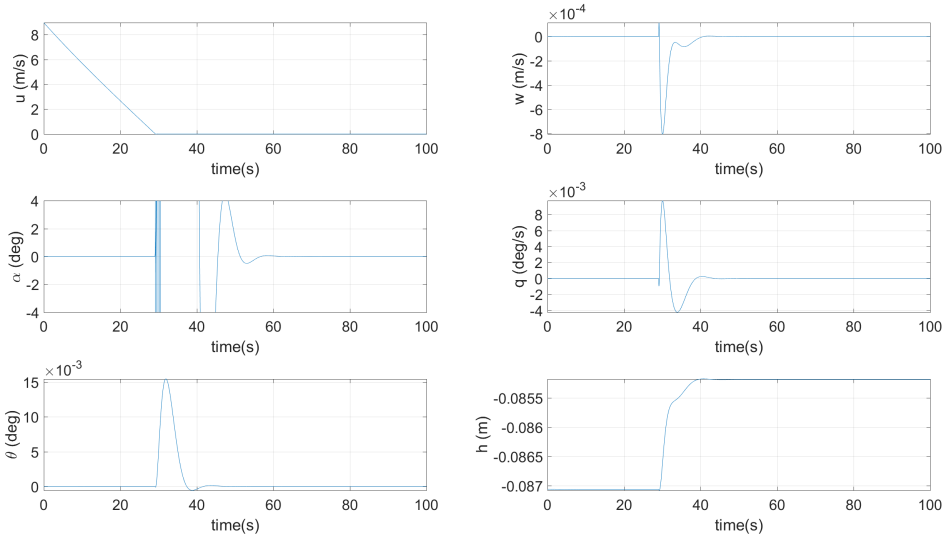

Figure 4.19: State of hybrid vehicle during backward transition to hover.

verse thrust. At 28 seconds forward velocity reaches zero and the hover controller is turned on. The forward velocity is then controlled to zero for the remaining time.

Vertical Velocity (w): The vertical velocity remains at zero until the switch is made. The rapid upward tilt creates momentary jump in vertical velocity due to thrust.

Euler Angle(θ): Theta remains at zero until the switch occurs. The theta angle then fluctuates upward due to an increase in forward vertical thrust as the tilt angle jumps to vertical. The variation is small in magnitude.

Altitude (h): There is a slight gain in altitude due to the forward movement of the tilt angle increasing the lift force. The altitude is then held constant.

States: Transition to Hover

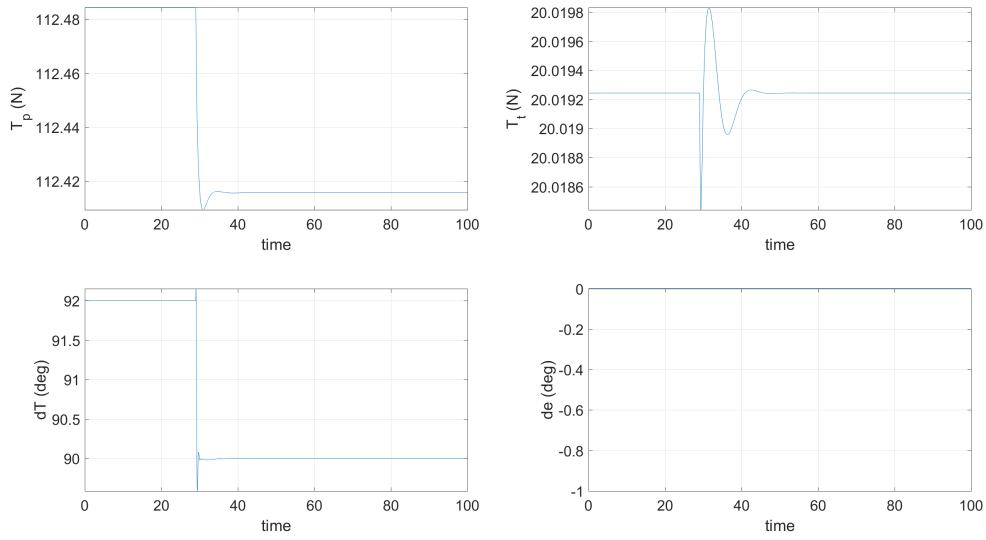

Figure 4.20: Inputs of hybrid vehicle during backward transition to hover.

The transition inputs can be seen in Figure 4.20.

Forward Thrust ($\mathbf{T_p}$): The forward thrust drops to meet the lift requirements. The thrust actuation changes slower than the tilt actuation and thus there is a moment of higher forward thrust inducing a pitching moment for a small amount of time.

Tail Thrust ($\mathbf{T_t}$): The tail thrust fluctuates to counter the forward thrust torque resulting from the tilt reduction. The tail thrust then increases to cancel the created theta angle.

Rotor Tilt (dT): The tilt rapidly adjust from its backward tilt of two degrees to a vertical orientation causing the forward propulsion to be slightly more than what is necessary for equilibrium.

Controller Effectiveness of Hover to Transition

Re-hovering following a decrease in speed to zero. There are slight fluctuations in state and input but variation is small in magnitude. The tilt angle quickly converting from two degrees past vertical to vertical causing a slight impulse in altitude and theta. This jump is very small an magnitude and acceptable.

The switch from transition to hover is now completed and an optional descent or climb command can be issued. All states remained stable and all inputs remained within their respective limitations. The transition and hover controllers have met their goals, and the switch has occurred as desired.

4.5 Total Flight

4.5.1 Total Flight:Unloaded and no CG Variation

The total flight of the hybrid craft can be seen in Figure 4.21.

The transition portions are as described above. All states are stable, all inputs are within their respective limitations and the respective controller goals are met.

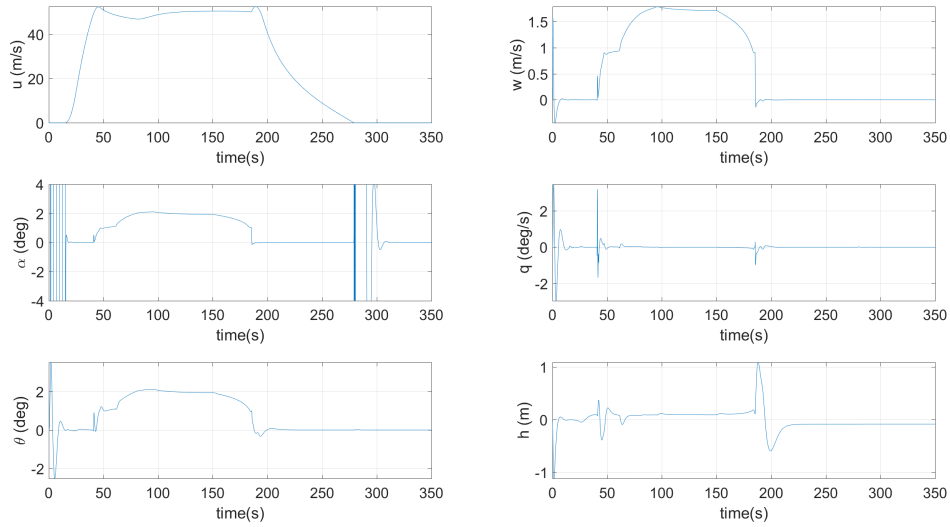

Figure 4.21: States of hybrid vehicle during a full forward and backward transition flight.

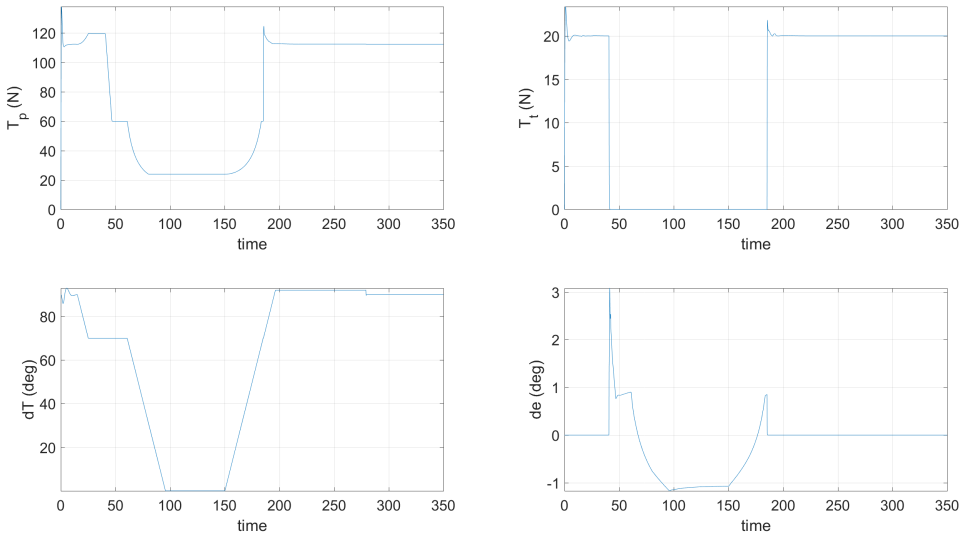

Figure 4.22: Inputs of hybrid vehicle during a full forward and backward transition flight.

4.5.2 Total Flight:Loaded and CG Variation

An overall of the total flight of the hybrid craft with a 4.5 kg payload and a CG variation of 0.05 m can be seen in Figure 4.23.

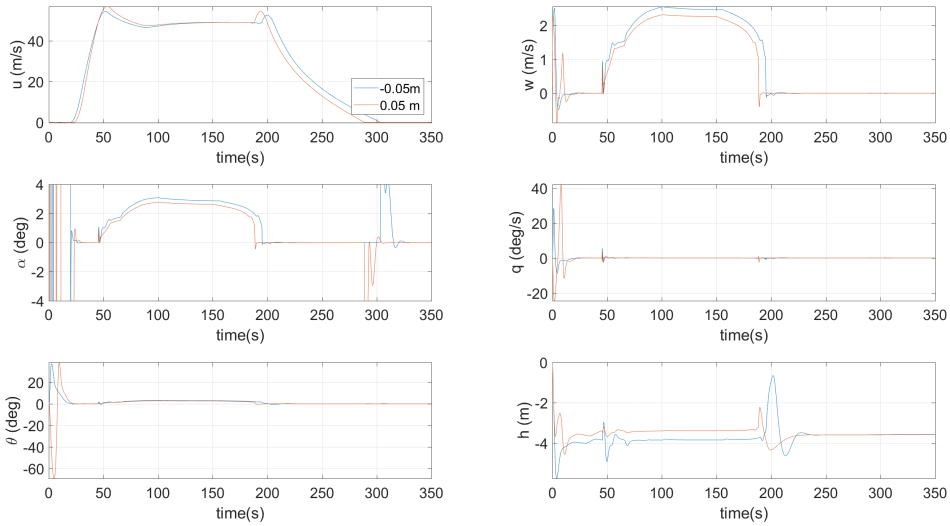

Figure 4.23: States of hybrid vehicle during a full forward and backward transition flight with loading and CG variation.

With loading and CG variation, the controller performs similarity to the unloaded case. The difference generally appears in the form of varied switching times and larger magnitudes of state perturbation. A slight off set in time is the result of varied switching times due to CG variation causing settling time differences.

The forward motion of the CG causes the largest initial disturbance. The disturbance can be seen by the large theta angle that appears near three seconds. The remaining states and inputs have larger magnitudes but remain stable. The inputs are within plausible domains. These disturbances are discussed in the hover section of results. The gain of altitude is in

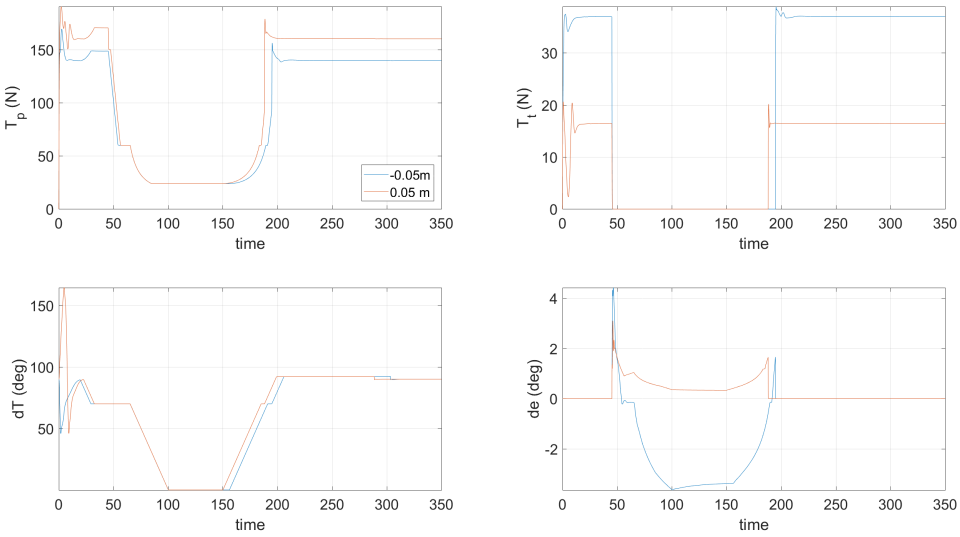

Figure 4.24: Inputs of hybrid vehicle during a full forward and backward transition flight with loading and CG variation.

11

general higher with the increased mass and CG variation. The backward motion CG variation causes the highest altitude gain. The gain occurs at the moment of forward controller to transition controller switching, approximately 190 seconds. The increased altitude is due to the decreased stability in aerodynamic pitch stability. Shifting the CG backward decreases the tail effectiveness and the result is more deviation of theta that in turn creates a higher altitude gain when switch occurs. The largest fluctuation is now three meters peak to peak over the course of fifteen seconds. The magnitude of deviation is large but the deviation is a positive altitude gain, as opposed to a loss of altitude and over a time period of around 15 seconds. It stabilizes out and returns to effectively no gain in altitude once equilibrium of the transmission controller is achieved. All states remain stable and all inputs remain within their limitations. The controllers perform successfully with both added mass and CG variation.

Chapter 5

CONCLUSION

In the above thesis the modeling and control of a tilt rotor tri-copter with a fixed wing assembly is theorized, simulated, and discussed. A 3 DOF model was determined and simulated with non-linear equations to model the dynamics of a hybrid craft. A control strategy was devised with control goals set to meet the transition strategy. The controllers were then synthesized via a means of full state control, integral action, gain scheduling, and classical flight control techniques. The controllers were merged together by means of logic switches and memory input based transitions. The final controller demonstrated viable control of the conceptual model throughout a forward and backward transition. All states were stabilized during the flight and the inputs applied were within acceptable ranges set forth at the beginning of the paper. The controller is a simple and acceptable means to provide transition control for a fixed wing tri-copter.

BIBLIOGRAPHY

[1] Dugan, Daniel C. "Trust control of VTOL aircraft part deux." (2014).

[2] Bolkcom, C. "CRS Report for Congress. V-22 Osprey Tilt-Rotor Aircraft." Congressional Research Service, Fort Belvoir, VA, United States of America (2004).

[3] Zhang, Chunhua, and John M. Kovacs. "The application of small unmanned aerial systems for precision agriculture: a review." Precision agriculture 13.6 (2012): 693-712.

[4] Yuan, Chi, Zhixiang Liu, and Youmin Zhang. "UAV-based forest fire detection and tracking using image processing techniques." Unmanned Aircraft Systems (ICUAS), 2015 International Conference on. IEEE, 2015.

[5] Gundlach, John, et al. "Rail recovery system for aircraft." U.S. Patent No. 9,010,683. 21 Apr. 2015.

[6] Van Nieuwstadt, Michiel J., and Richard M. Murray. "Rapid hover-to-forward-flight transitions for a thrust-vectored aircraft." Journal of Guidance, Control, and Dynamics 21.1 (1998): 93-100.

[7] Maqsood, Adnan, and Tiauw Hiong Go. "Optimization of hover-to-cruise transition maneuver using variable-incidence wing." Journal of Aircraft 47.3 (2010): 1060-1064.

[8] Bapst, Roman, et al. "Design and implementation of an unmanned tail-sitter." Intelligent Robots and Systems (IROS), 2015 IEEE/RSJ International Conference on. IEEE, 2015.

[9] Marchini, Brian Decimo. Adaptive control techniques for transition-to-hover flight of fixed-wing UAVS. Diss. California Polytechnic State University San Luis Obispo, 2013.

[10] Hernandez-Garcia, Rogelio G., and H. Rodriguez-Cortes. "Transition flight control of a cyclic tiltrotor uav based on the gain-scheduling strategy." Unmanned Aircraft Systems (ICUAS), 2015 International Conference on. IEEE, 2015.

[11] Yanguo, Song, and Wang Huanjin. "Design of flight control system for a small unmanned tilt rotor aircraft." Chinese Journal of Aeronautics 22.3 (2009): 250-256.

[12] Ta, Duc Anh, Isabelle Fantoni, and Rogelio Lozano. "Modeling and control of a tilt tri-rotor airplane." American Control Conference (ACC), 2012. IEEE, 2012.

[13] Papachristos, Christos, Kostas Alexis, and Anthony Tzes. "Model predictive hovering-translation control of an unmanned tri-tiltrotor." Robotics and Automation (ICRA), 2013 IEEE International Conference on. IEEE, 2013.

[14] Dickeson, Jeffrey J., et al. "Robust LPV H∞ gain-scheduled hover-to-cruise conversion for a tilt-wing rotorcraft in the presence of CG variations." Decision and Control, 2007 46th IEEE Conference on. IEEE, 2007.

[15] Chowdhury, Arindam Bhanja, Anil Kulhare, and Gaurav Raina. "A generalized control method for a Tilt-rotor UAV stabilization." Cyber Technology in Automation, Control, and Intelligent Systems (CYBER), 2012 IEEE International Conference on. IEEE, 2012.

[16] Muraoka, Koji, Noriaki Okada, and Daisuke Kubo. "Quad tilt wing vtol uav: Aerodynamic characteristics and prototype flight." AIAA Infotech@ Aerospace Conference and AIAA Unmanned... Unlimited Conference. 2009.

[17] Sato, Masayuki, and Koji Muraoka. "Flight Controller Design and Demonstration of Quad-Tilt-Wing Unmanned Aerial Vehicle." Journal of guidance, control, and dynamics 38.6 (2014): 1071-1082.

[18] Ferguson, Samuel W. "A Mathematical Model for Real Time Flight Simulation of a Generic Tilt-Rotor Aircraft." NASA CR-166536 (1988).

[19] Harendra, P. B., et al. "V/STOL tilt rotor study. Volume 5: A mathematical model for real time flight simulation of the Bell model 301 tilt rotor research aircraft." (1973).

[20] Liu, Zhong, et al. "Control techniques of tilt rotor unmanned aerial vehicle systems: A review." Chinese Journal of Aeronautics (2016).

[21] Papachristos, Christos, Kostas Alexis, and Anthony Tzes. "Linear quadratic optimal trajectory-tracking control of a longitudinal thrust vectoring-enabled unmanned Tri-TiltRotor." Industrial Electronics Society, IECON 2013-39th Annual Conference of the IEEE. IEEE, 2013.

[22] ONER, Kaan. Mathematical modeling and vertical flight control of a tilt-wing UAV. Turk J Elec Eng and Comp Sci, Vol.20, No.1, 2012

[23] Oner, Kaan Taha, et al. "Mathematical modeling and vertical flight control of a tilt-wing UAV." Turkish Journal of Electrical Engineering and Computer Sciences 20.1 (2012): 149-157.

[24] Senkul, Fatih, and Erdinc Altug. "Adaptive control of a tilt-roll rotor quadrotor UAV." Unmanned Aircraft Systems (ICUAS), 2014 International Conference on. IEEE, 2014.

[25] Johnson, Eric N., et al. "Flight test results of autonomous fixed-wing UAV transitions to and from stationary hover." Proceedings of the AIAA Guidance, Navigation, and Control Conference Exhibit, Monterey, CO. 2006.

[26] Gutierrez, Luis B., George Vachtsevanos, and Bonnie Heck. "An approach to the adaptive mode transition control of unmanned aerial vehicles." American Control Conference, 2003. Proceedings of the 2003. Vol. 5. IEEE, 2003.

[27] Lu, Ke, et al. "Modeling and control of tilt-rotor aircraft." Control and Decision Conference (CCDC), 2016 Chinese. IEEE, 2016.

[28] Chao, Dai, Bai Huihui, and Zeng Jianping. "Nonlinear stabilization control of tilt rotor UAV during transition flight based on HOSVD." Guidance, Navigation and Control Conference (CGNCC), 2016 IEEE Chinese. IEEE, 2016.

[29] Xili, Yang, Fan Yong, and Zhu Jihong. "Transition flight control of two vertical/short takeoff and landing aircraft." Journal of guidance, control, and dynamics 31.2 (2008): 371-385.

[30] Schmidt, David. Modern flight dynamics. McGraw-Hill Higher Education, 2012.

[31] Smetana, Frederick O., Delbert Clyde Summey, and W. Donald Johnson. Riding and Handling Qualities of Light Aircraft: A Review and Analysis. National Aeronautics and Space Administration, 1972.

[32] Nise, Norman S. CONTROL SYSTEMS ENGINEERING, (With CD). John Wiley and Sons, 2007.

[33] Rugh, Wilson J., and Jeff S. Shamma. "Research on gain scheduling." Automatica 36.10 (2000): 1401-1425.

[34] Acquatella, Paul, Wim van Ekeren, and Qi Ping Chu. "PI (D) tuning for Flight Control Systems via Incremental Nonlinear Dynamic Inversion." arXiv preprint arXiv:1701.08981 (2017).

[35] Hespanha, Joao P. Linear systems theory. Princeton university press, 2009.

[36] Stengel, Robert F. Optimal control and estimation. Courier Corporation, 2012.

[37] Chao, Dai, Bai Huihui, and Zeng Jianping. "Nonlinear stabilization control of tilt rotor UAV during transition flight based on HOSVD." Guidance, Navigation and Control Conference (CGNCC), 2016 IEEE Chinese. IEEE, 2016.

[38] Rysdyk, Rolf T., and Anthony J. Calise. "Adaptive model inversion flight control for tilt-rotor aircraft." Journal of guidance, control, and dynamics 22.3 (1999): 402-407.

[39] Johnson, Eric N., et al. "Flight-test results of autonomous airplane transitions between steady-level and hovering flight." Journal of guidance, control, and dynamics 31.2 (2008): 358-370.